HHS Public Access

Author manuscript

Cell Host Microbe. Author manuscript; available in PMC 2022 May 12.

Published in final edited form as:

Cell Host Microbe. 2021 May 12; 29(5): 777–791.e6. doi:10.1016/j.chom.2021.03.003.

Bacteria Induce Skin Regeneration via IL-1β Signaling

Gaofeng Wang[1,2], **Evan Sweren**[1], **Haiyun Liu**[1], **Eric Wier**[1], **Martin P. Alphonse**[1], **Ruosi Chen**[1,2], **Nasif Islam**[1], **Ang Li**[1], **Yingchao Xue**[1], **Junjie Chen**[3], **Seungman Park**[3], **Yun Chen**[3], **Sam Lee**[1], **Yu Wang**[1], **Saifeng Wang**[1], **Nate K. Archer**[1], **William Andrews**[4], **Maureen A. Kane**[4], **Erika Dare**[1], **Sashank K. Reddy**[1,5], **Zhiqi Hu**[2], **Elizabeth A. Grice**[6], **Lloyd S. Miller**[1,7], **Luis A. Garza**[1,8,9,*]

[1]Department of Dermatology, Johns Hopkins University School of Medicine, Baltimore, MD 21210, USA.

[2]Department of Plastic and Aesthetic Surgery, Nanfang Hospital of Southern Medical University, Guangzhou, Guangdong Province 510515, China.

[3]Department of Mechanical Engineering, Johns Hopkins University, Baltimore, MD 21210, USA.

[4]Department of Pharmaceutical Sciences, School of Pharmacy Mass Spectrometry Center, University of Maryland, MD 21201, USA.

[5]Department of Plastic and Reconstructive Surgery, Johns Hopkins School of Medicine, Baltimore, MD 21287, USA

[6]Department of Dermatology and Microbiology, Perelman School of Medicine, University of Pennsylvania, Philadelphia, PA 19104, USA.

[7]Immunology, Janssen Research and Development, 1400 McKean Road, Spring House, PA 19477, USA.

[8]Department of Cell Biology, Johns Hopkins University School of Medicine, Baltimore, MD 21210, USA.

[9]Lead Contact.

SUMMARY

Environmental factors that enhance regeneration are largely unknown. The immune system and microbiome are attributed roles in repairing and regenerating structure but their precise interplay is unclear. Here, we assessed the function of skin bacteria in wound healing and Wound Induced Hair

*Correspondence to: LAG@jhmi.edu.

Author contributions: G.W., H.L., and L.A.G. designed the study and experiments; G.W., E.S., and L.A.G. wrote the manuscript; G.W. performed the experiments and analyzed the data; H.L., E.S., E.W., M.A., N.I., A.I., Y.X., R.C., J.C.,Y.C., S.L., Y.W., N.A., A.W., K.M., E.D., Z.H., E.G., L.M., and L.A.G. participated in performing experiments, provided intellectual expertise, and and/or helped to interpret experimental results; G.W. assisted with microarray and RNA-seq data analysis, isolated, cultured keratinocytes. G.W. and H.L. performed confocal microscopy and bacteria culture; G.W. and E.S. analyzed human skin biopsies; G.W. analyzed the 16S rRNA data and performed wounding studies and GF experiments.

(Current affiliation. All work performed at prior affiliation[1])

follicle Neogenesis (WIHN), a rare adult organogenesis model. WIHN levels and stem cell markers correlate with bacterial counts, being lowest in germ-free (GF), intermediate in conventional specific pathogen free (SPF), and highest in wild-type mice, even those infected with pathogenic *Staphylococcus aureus*. Reducing skin microbiota via cage changes or topical antibiotics decreased WIHN. Inflammatory cytokine IL-1β and keratinocyte-dependent IL-1R-MyD88 signaling are necessary and sufficient for bacteria to promote regeneration. Finally, in a small trial, a topical broad-spectrum antibiotic also slowed skin wound healing in adult volunteers. These results demonstrate a role for IL-1β to control morphogenesis and support the need to reconsider routine applications of topical prophylactic antibiotics.

Graphical Abstract

The influence of environment factors on skin regeneration remains unclear. Wang et al find that skin bacteria induce IL1β signaling and activate keratinocytes via a pathway requiring IL1R/Myd88 to stimulate hair follicle regeneration and wound healing.

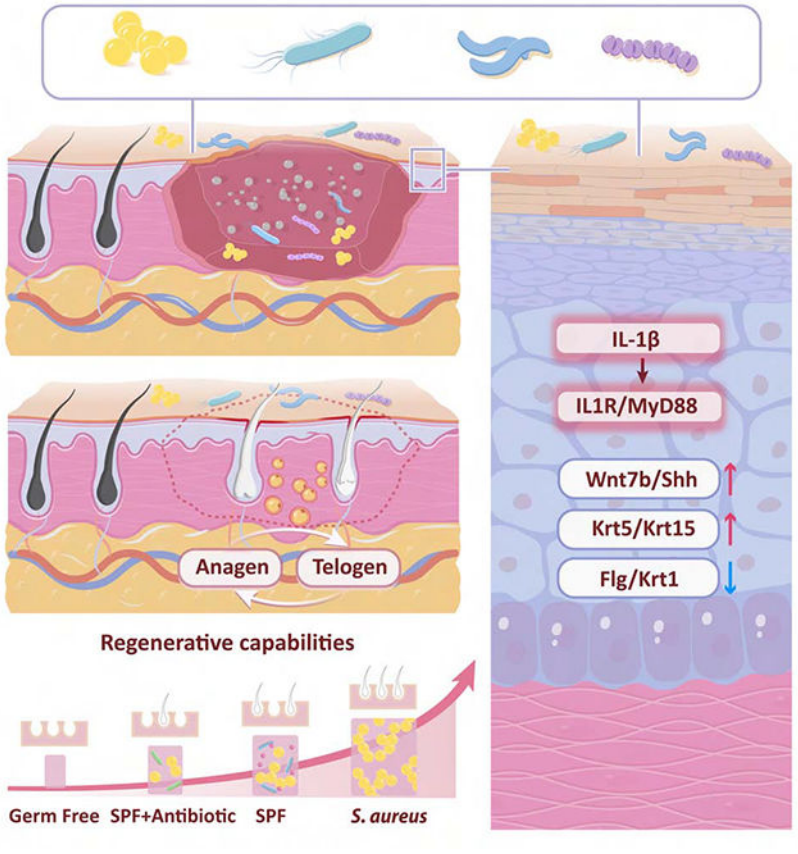

INTRODUCTION

Several vertebrates, including salamanders and zebrafish, have strong regenerative abilities, which have been linked to immune cell activation. Adult organogenesis, however, in mammals is rare. Among these different contexts of regeneration, the immune system and the microbiome have varying roles to repair and regenerate structure and function (Godwin

et al., 2013) (Kyritsis et al., 2012) (Taniguchi et al., 2015) (Lee et al., 2017). However, whether beneficial aspects of inflammation extend to wholesale infection and what the specific relationship between immune inflammation response and skin regeneration remains unknown.

Wound-induced hair neogenesis (WIHN) is a rare model of mammalian organ regeneration in rabbits and mice wherein large full-thickness skin defects induce hair follicle regeneration with complete stem cell pools, specialized vascular and nerve supports, sebaceous glands, and surrounding fat cells (Ito et al., 2007; Kim et al., 2019; Plikus et al., 2017). This occurs through the migration of hair follicle and epidermal stem cells from the wound edge to the wound center (Ito et al., 2005; Ito et al., 2007; Park et al., 2017) to coordinate the early stages of wound healing. At least a subset of stem cells maintain their lineage during migration (Ito et al., 2005; Joost et al., 2018; Park et al., 2017) to populate the regenerative hair follicle epithelial placodes under the activation of classical WNT signaling to initiate morphogenesis (Ito et al., 2007). During the development of the hair germ, an essential SHH signal is induced both in the epithelial placodes and also the dermal papilla to continue morphogenesis (Lim et al., 2018). Coincident with these effects, the pro-regeneration influence of skin immune microenvironment has been confirmed (Gay et al., 2013; Lee et al., 2017; Wang et al., 2017).

The remarkable regenerative capacity of fetal tissue is often attributed to its immature immune system and the deleterious effects of immune reactions on regeneration. However, in the mature immune system, the relationship between inflammation signals and regeneration may be different (Kathju et al., 2012; Larson et al., 2010). Damage associated molecular patterns (DAMPs) signal tissue injury to prime the regenerative process; but precisely how these factors influence stem cells' fate and hair follicle neogenesis is not fully understood (Ito et al., 2007). Interestingly, previous studies reported a correlation between wound size and regenerative ability, wherein larger wounds induce stronger regeneration (Gay et al., 2020; Ito et al., 2007; Lim et al., 2018). We thus hypothesize that a stronger inflammatory response may activate a more robust regenerative response, despite evidence to the contrary (Larson et al., 2010; Wulff et al., 2012).

The local microbiome is known to have multiple benefits to the host, for example promotion of intestinal regeneration (Abo et al., 2020; Wu et al., 2020). Yet, topical prophylactic antibiotic use is a mainstay by the public even in small uninfected skin wounds. We queried if indeed the skin microbiome promotes healing but also if this extended to a pathogenic abundance of bacteria. To do so, we tested three levels of bacterial burden to assess WIHN and study the relationship between skin microbiota and skin regeneration. We find that the bacterial burden of mouse skin positively correlates with and stimulates regeneration through IL1β, and this holds true in a trial in human subjects as well.

RESULTS

Commensal Microbiota induce hair regeneration

To test the role of the microbiome in regeneration, we wounded germ-free (GF) mice through a GF bubble (Figure S1A) or performed standard wounds on normal specific

pathogen-free (SPF) mice and assessed WIHN levels. WIHN of GF mice is significantly lower (fold= −17.9, p=1.9×10^{-6}) (Figure 1A). We confirmed that GF mice had lower α-diversity and clustered β-diversity (Figures 1B and 1C) and note *Pseudomonas* and *Staphylococcus* are the dominant bacteria in SPF mice skin (Figure S1B). Therefore, lower bacterial quantity and diversity correlates with lower regeneration.

To characterize the tissue changes above, we analyzed gene expression of wounded GF and SPF mice skins on ~Wound Day 12 (WD12), which is also scab-detach day 0 (SD0), the day where the new epithelium completes coverage of the wound and the scab is released but before morphogenesis or regeneration has begun. Microarray results demonstrate an elevation of morphogenesis and immune activation transcripts in SPF mice (Figure 1D, and Figure S1C). Conversely, transcripts for keratinocyte differentiation, keratinization, and cornified envelope are significantly higher in GF mice (Figure 1D). Previous studies have shown that prior to hair regeneration, increased stemness genes in the wound bed allow prolonged maintenance of dedifferentiated keratinocytes and ultimate hair follicle cell differentiation and hair follicle neogenesis. These include higher levels of stem cell markers, such as Krt15, and regeneration signals, such as Wnt7b, Tgfb1, and β-Catenin, and lower levels of keratinocyte differentiation markers, such as Flg and Krt1 (Ito et al., 2007; Kim et al., 2019; Nelson et al., 2015; Qi et al., 2018). In confirmatory qRT-PCR, the stem cell marker *Krt15* and regeneration signals *Wnt7b* and *Tgfb1* are significantly higher in SPF mice than in GF mice (Figure 1E). In contrast, the keratinocyte differentiation markers *Krt1* and *Flg* are significantly elevated in GF mice (Figure 1E) (Kim et al., 2019). Immunofluorescence staining confirms these changes with higher levels of β-Catenin in SPF than in GF mice (Figure 1F). We also observe delayed wound healing in GF mice on WD5, suggesting SPF mice's skin biome promotes healing ability (Figure 1G). Consistent with previous studies of immune cells' positive effect on WIHN (Chu et al., 2019; Gay et al., 2013; Kasuya et al., 2018; Scharschmidt et al., 2017; Wang et al., 2017), M2 macrophages, CD4+T cells, and γδT cells are significantly higher in the SPF mice wound bed than in GF mice (Figure S2A and S2B). These results are consistent with the greater regeneration seen in SPF over GF mice.

We next queried if the decreased regeneration in GF mice was a function of immune education and was irreversible, or instead if the GF mice regeneration could be rescued with microbial exposure. To do so, we transferred GF mice to an SPF facility after wounding to co-house the GF mice with SPF mice and transfer SPF microbiota to the formerly GF mice (Archer et al., 2019). Consistent with reversibility, co-housed GF mice increases WIHN to levels significantly higher than control GF mice (fold= 8.0, p=4.7×10^{-5}) (Figure 1H). This functional evidence supports a model where local skin resident microbiota promote regeneration during wound healing.

Microbiota dysbiosis alters regeneration capacity.

In vivo assays such as WIHN can have variability; for example, the result might be different even using the same mouse strain among different academic institutions. Given that previous studies demonstrated how cage bedding cleaning frequencies affect the microbiota of mice skin (SanMiguel et al., 2017) and our results above, we hypothesized cage change frequency

would also alter regeneration. We compared two groups of SPF mice: change every day (CED) and never change (NC). NC mice were similarly perturbed without changing cage to reduce potential confounders of stress and sleep cycle disturbance. As expected, WIHN of NC mice is significantly higher than CED mice (fold= 3.7, p=3.2×10^{-4}) (Figure 2A). Also, consistent with our results on GF mice, α and β-diversity are both consistent with a decreased microbiome in CED compared to NC mice (Figure 2B and 2C). Next, we analyzed the taxonomy of the microbiome of these mice and observe *Staphylococcus* and *Streptococcus* are somewhat more elevated in NC mice (Figure 2D and Figure S2C). These findings indicate that environmental changes can modify regeneration ability, possibly via the microbiome.

For loss of function, we explored if topical antibiotics that reduce resident microbiota of SPF mouse skin would inhibit WIHN. Previous studies have shown that topical Neosporin, a commonly used over the counter triple-antibiotic ointment containing bacitracin, neomycin and polymyxin, reduces resident skin microbiota and inhibits bacterial repopulation (Hendley and Ashe, 2003). A very recent report also demonstrated that Neosporin inhibits mouse wound healing (Di Domizio et al., 2020). Given this overlap, we thus applied Neosporin on wounded SPF mice and compared WIHN levels against SPF mice treated with vehicle. Consistent with our results above, Neosporin application dramatically inhibits WIHN (fold=−7.9, p=8.4×10^{-5}) (Figure 2E). These results confirm the environmental role of commensal microbiota to promote regeneration.

S. aureus promotes regeneration

Given the importance of the commensal microbiome, we hypothesized that even pathogenic skin infections might enhance WIHN. Bacteria were injected subcutaneously to localize its effects on the skin and eliminate potential ingestion/intestinal microbiota changes. We first performed a bioinformatics analysis of the gene expression differences within multiple previous models of high and low WIHN to query for any signature that might predict the effect of skin infection on WIHN. Interestingly, RNA-seq gene ontology analysis demonstrates that multiple instances of high regeneration are associated with gene signatures of bacterial skin infection (Kim et al., 2019) (Figure 3A to 3C). For example, in *Rnasel*$^{-/-}$ mice (high WIHN), which we discovered have enhanced regeneration based on our previous microarray analysis comparing high and low WIHN mice strains (Nelson et al., 2013), gene transcripts involved in *S. aureus* infection are the second most significant upregulated category (Figure 3A). In an analysis of WT mice (high WIHN) versus *Rara*$^{-/-}$ mice (low WIHN) (Kim et al., 2019), gene transcripts involved in *S. aureus* infection rank seventh (Figure 3B). In a third analysis of the proteome comparing the wound center (high WIHN) versus wound periphery (low WIHN) (Ito et al., 2007; Kim et al., 2019; Lim et al., 2018; Plikus et al., 2017), the *S. aureus* infection category ranks third (Figure 3C). These disparate experimental contexts converge to suggest that *S. aureus* infection response correlates with high WIHN. To further explore what signals are involved in *S. aureus* infection pathways, we searched for genes enriched in this category. We find that most of the genes are complement signals, which are known to play an innate immune role in acute inflammation (Figure S3A) (Walport, 2001). We also find that the IL-1 family expression correlates to high WIHN; higher in *Rnasel*$^{-/-}$ mice and lower in *Rara*$^{-/-}$ mice (Figure S3B and S3C).

This indicates that the innate immunity and IL-1 family activation signals may be important for hair follicle regeneration.

To begin testing the effect of *S. aureus* exposure on regeneration, we first tested its effect on hair follicle cycling. *S. aureus* induces the surrounding hair follicle to transfer from the resting telogen to the growing anagen phase (Figure 3D). Next, to assess their role in WIHN, bioluminescent *S. aureus* and *S. epidermidis* (1×10^7 CFU/each) were separately injected into the early wounds of SPF mice. Compared to control, *S. epidermidis* significantly increases WIHN by 1.5 times (p=0.014); moreover, *S. aureus* increases WIHN by 3.3 times ($p=7.5\times10^{-5}$) (Figure 3E). To determine whether the de novo hair follicles induced by *S. aureus* follow the developmental pattern of hair follicles during the embryonic period, we tracked the morphology and markers of hair follicles at different time points after wounding. We find that from WD14-WD27, *S. aureus* promotes wound bed stem cells to develop hair germs and complete hair follicle structures with sebaceous glands (Figure 3F). Krt17 is also highly expressed in the hair germ during this period. Wnt7b and β-Catenin are highly expressed in hair matrix cells of the hair bulb and hair follicle stem cells of the hair bulge (Figure 3F). This confirms that the neogenic hair follicles induced by bacteria follow the pattern of embryonic hair follicle development. Importantly, the greater stimulation of WIHN with *S. aureus* compared to *S. epidermis* correlates with their longevity in the skin. *S. epidermidis* abundance decreases by 90% after 2 days of injection, while *S. aureus* requires 7 days for an equivalent 90% reduction (Figure 3G), consistent with previous reports (Archer et al., 2019). We subsequently tested a variety of gram-positive and negative bacteria and find they similarly induce WIHN in a somewhat dose-dependent manner (Figure S4A to S4E). Together, these data suggest that stronger and more persistent inflammation signaling stimulates higher WIHN, likely with heterogeneous contributions from different bacterial species.

To characterize the above changes, we analyzed mRNA and protein expression changes. Consistent with our previous findings, *S. aureus* infection is associated with greater inflammation, more development growth factors, and less differentiation, whereas controls show the reverse (Figure 3H and 3I; Figure S4F and S4G). Microarray results confirm an elevation of immune cell activation transcripts in *S. aureus* treated mice (Figure 3J and Figure S4H). Although some hair follicle development genes are down-regulated in *S. aureus* injected skin, these genes are terminal differentiation markers, like *Krt27*, *Krt83*, *Krt25*, *Krt71*, which participate in the formation of the hair shaft (Figure 3J). These results suggest that *S. aureus* inhibits keratinocyte differentiation to likely promote stem cell maintenance during regeneration.

Given that co-housing rescues low WIHN in GF mice, we next queried if co-housing with *S. aureus* infected animals could also improve WIHN in their uninfected cage mates. Even without direct injection and likely without any modification of intestinal bacteria, WIHN of co-housed mice is significantly increased (fold=2.7, $p=7.2\times10^{-5}$) (Figure 3K). In this context, α-diversity decreases, given that *S. aureus* inhibits other bacteria, and β-diversity clustered (Figure 3L and 3M). As expected, co-housed and injected mice also possess significantly higher *Staphylococcus* burden than control mice (Figure 3N and Figure S5A). These results demonstrate that increasing epidermal exposure of *S. aureus* induces WIHN.

Regeneration induced by *S. aureus* requires MyD88 Signaling in Keratinocytes

We next investigated the mechanism of increased regeneration after *S. aureus* challenge. Given the central role of MyD88 in immune signaling (Liu et al., 2017; Miller et al., 2006), we first tested WIHN of *Myd88*$^{-/-}$ mice with or without *S. aureus* addition. *Myd88*$^{-/-}$ mice have markedly lower WIHN relative to WT mice, which cannot be rescued by *S. aureus* injection (fold=−19.3, p=8.8×10^{-6}) (Figure 4A). As expected, M2 macrophages and γδT cells are significantly lower in *Myd88*$^{-/-}$ mice wound beds than in WT (Figure S5B) (Chu et al., 2019; Gay et al., 2013; Kasuya et al., 2018; Scharschmidt et al., 2017; Wang et al., 2017). Significantly delayed wound closure speed in *Myd88*$^{-/-}$ relative to WT mice is also apparent (Figure 4B). This finding implicates and confirms Myd88 as essential for bacterial-induced WIHN and healing.

We next sought to define the cell type where Myd88 is required for regeneration. After wounding, we assessed WIHN levels of homozygous and heterozygous *LysM*^{cre} *X Myd88*$^{fl/fl}$ (myeloid cells) and *K14*^{cre} *X Myd88*$^{fl/fl}$ (keratinocytes) mice. For myeloid cells, both homozygotes (*Lym-Myd88*$^{-/-}$) and heterozygotes (*Lym-Myd88*$^{+/-}$) retain similar WIHN as WT mice. Enhanced WIHN can also be induced by *S. aureus* injection (Figure 4C), indicating that regeneration does not require Myd88 signaling in myeloid cells. However, WIHN of *K14-Myd88*$^{-/-}$ mice is significantly lower than WT mice and cannot be rescued by *S. aureus* injection (Figure 4C). These results suggest Myd88 signaling in keratinocytes is necessary for wound-induced regeneration and for bacteria-induced regeneration.

Although increasing skin bacteria does not rescue low WIHN of *Myd88*$^{-/-}$ and *K14-Myd88*$^{-/-}$ mice, we hypothesized that the lack of Myd88 might also modify the mouse epidermal microbiome given the slower wound closure speed noted above. We find that both *Myd88*$^{-/-}$ and *K14-Myd88*$^{-/-}$ mice have lower microbiome α-diversity than WT mice (Figure 4D). The proportion of *Pseudomonas* or *Streptococcus* increases, while other bacteria, including *Staphylococcus*, decrease in Myd88 deficient mouse skin (Figure 4E). These results are consistent with a previous study that shows *Myd88*$^{-/-}$ mice are susceptible to *Pseudomonas* and indicate the important roles of Myd88 in balancing and maintaining microbiome on wounded skin. (Villano et al., 2014).

IL-1β-IL-1R in Keratinocytes Is the Primary MyD88 Upstream Signal that Promotes Skin regeneration

To identify which signal is responsible for Myd88 to induce regeneration, we screened candidates based on our previous WIHN gene and protein screens (Kim et al., 2019; Nelson et al., 2015). We tested WIHN in *Tlr2*$^{-/-}$, *Il-1r*$^{-/-}$, and *Il-36r*$^{-/-}$ mice. *Tlr2*$^{-/-}$ mice display normal WIHN, while *Il-1r*$^{-/-}$ (fold=−9.5, p=2×10^{-4}) and *Il-36r*$^{-/-}$ mice (fold=−2.0, p=0.029) display lower WIHN (Figure 5A). This suggests that the TLR2 signal is not essential for regeneration but that the IL-1R and IL-36R signals play pro-regenerative roles. We next injected *S. aureus* into all three mutant mice. While *S. aureus* increases WIHN in *Tlr2*$^{-/-}$ (fold=1.9, p=1.6×10^{-3}) and *Il-36r*$^{-/-}$ mice (fold=3.2, p=4.5×10^{-3}), WIHN of *Il-1r*$^{-/-}$ mice remains inhibited and unaltered (Figure 5A). Our previous studies have shown that TLR3 signaling is important for hair follicle regeneration (Nelson et al., 2015). Also, studies

have shown that TLR3 signals are activated during bacterial infections and play a role in activating inflammation (Lai et al., 2009). We thus tested the expression of TLR3 in GF, SPF, PBS treated, and *S. aureus* treated mice. We find that TLR3 signaling is highly expressed in mice with higher bacterial load and better WIHN (Figure S5C). However, *S. aureus* rescues *Tlr3*$^{-/-}$ mice's low WIHN, which suggests that bacteria induced WIHN is TLR3 signaling independent (Figure S5D). This indicates that *S. aureus* uniquely induces regeneration by way of IL-1R signaling.

Though bacteria cannot rescue the regenerative ability of *Il-1r*$^{-/-}$ mice, we again questioned how the absence of IL-1 signaling might modify commensals. The microbiome diversity of *Il-1r*$^{-/-}$ mice is not significantly different from that of WT mice, though it does trend lower (Figure 5B). More clearly, similar to *Myd88*$^{-/-}$ mice, *Streptococcus* and *Pseudomonas* increase while other bacteria, including *Staphylococcus*, decrease on *Il-1r*$^{-/-}$ mice skin, indicating an analogous role of IL-1 signaling to balance and maintain the microbiome on wounded skin.

We next investigated which IL-1R ligands might promote WIHN by comparing the expression of interleukins and chemokines in mRNA transcripts from high versus low WIHN groups: SPF versus GF; and *S. aureus* versus Vehicle, respectively (Figure 5C and 5D). In both experimental contexts, *Il-1β* gene expression most consistently correlates with high WIHN (Figure 5C and 5D). We next measured the expression of *Il-1α* and *Il-1β* at different time points during wounding to further define their roles. Again, *Il-1β* levels best correlate with high WIHN (Figure 5E). These results suggest that during wounding, IL-1β signaling rather than IL-1α promotes regeneration.

To define the source of IL-1β in the wound bed, we stained mouse SD0 wound bed with IL-1β co-stained with F4/80 as a macrophage marker. Previous studies have shown that the main source of IL-1β is myeloid, especially macrophages (Huang et al., 2019; Ishida et al., 2020). Also, studies have shown that in inflamed skin and scars, IL-1β is highly expressed in keratinocytes (Cai et al., 2019; Liao et al., 2017; Salgado et al., 2012). Our results show that though absent in controls (no primary antibody and *IL-1β*$^{-/-}$ mice), IL-1β is highly expressed in both keratinocytes and macrophages (Figure S6G, S6H and 6D).

To functionally test the importance of IL-1β, we examined its effects in vitro and in vivo. First, given the increase in developmental growth factors and decrease in differentiation with bacteria in wounding, we tested the effect of IL-1β on human keratinocytes. Consistent with those results, the rhIL-1β treated group significantly increases the expression of *WNT7B*, *SHH*, *KRT7,* and *LEF1* but significantly reduces the expression of *KRT1* and *FLG* in a concentration-dependent manner (Figure 5F) (Zhou et al., 2019). Next, we applied exogenous rmIL-1α, rmIL-1β, or heat-kill *S. aureus* to wounded mice. Heat-killed bacteria and Il-1α fail to promote WIHN (Figure 5G). However, rmIL-1β enhances WIHN (fold=2.5, p=0.015) (Figure 5G).

To compare loss of function models to the above gain of function tests, we wounded *Il-1α*$^{-/-}$ and *Il-1β*$^{-/-}$ mice treated with or without *S. aureus*. *Il-1α*$^{-/-}$ mice regenerate normally, and *S. aureus* stimulates WIHN (fold=2.3, p=0.028) (Figure 5H). In contrast, WIHN of *Il-1β*$^{-/-}$

mice is significantly lower than that of WT mice (fold=−7.0, p=0.001) and cannot be increased with *S. aureus* injection (Figure 5H). Consistent with the results after body wide deletion, mice with a keratinocyte specific deletion of IL-1R (*K14-Il-1r*$^{-/-}$) also exhibit low WIHN (fold=−7.7, $p=8.9\times10^{-4}$), which *S. aureus* fails to stimulate (Figure 5H). Consistent with *Myd88*$^{-/-}$ mice, the wound closure speed in *Il-1β*$^{-/-}$ mice is significantly delayed compared to WT mice (Figure 5I).

Since endogenous IL-1β is essential for hair follicle regeneration and accelerated skin reepithelialization as shown above, we next measured if IL-1β loss modifies the tensile strength of the healed wound bed. For both WT and *Il-1β*$^{-/-}$ mice, tensile strength of healthy skin is significantly higher than that of wound bed. However, there is no significant difference between the strength of wound bed of WT and *Il-1β*$^{-/-}$ mice (Figure 5J). These findings indicate that bacterial enhanced regeneration and healing is through endogenous IL-1β stimulation of a keratinocyte IL-1R-MyD88 pathway, while it has no effect on the strength of the whole skin, likely more related to collagen production and fibroblasts.

To confirm the effects of IL-1β in vitro and in vivo, we tested IL-1β on keratinocytes derived from WT mice or *Il-1r*$^{-/-}$ and *Myd88*$^{-/-}$ mice. We find that the effects of IL-1β on increasing developmental growth factors and inhibiting differentiation depends on expression of IL-1R and Myd88 (Figure 5K). In this vein, exogenous rmIL-1β cannot rescue WIHN of *K14-Myd88*$^{-/-}$ mice (Figure 5L). These results are consistent with a model where bacteria promote regeneration through IL-1β-IL-1R-MyD88 signaling in keratinocytes.

Given γδT cells' indispensable role in regeneration (Gay et al., 2013) and our findings of increased γδT cells in high WIHN mice, we next explored the role of adaptive immunity in our model (Figure S2A and S5B). Interestingly, in published reports, *S. aureus* induces skin γδT cells production of IL-17A after activating Myd88 signaling, and IL-17A promotes stemness of both keratinocyte and mucosal cells (Archer et al., 2019; Ekman et al., 2019; Zhang et al., 2018). We likewise observe higher IL-17A production from γδT cells in *S. aureus* treated mice wound beds (Figure S6A). We thus isolated T cells from the secondary lymph nodes of WT mouse skin and injected them into *Myd88*$^{-/-}$ mice wound beds to determine if IL-1β-IL1R-Myd88 signaling is γδT cells and IL-17 dependent. However, T cells from WT mice cannot rescue low WIHN of *Myd88*$^{-/-}$ mice (Figure S6B) nor does treatment of HFKC with rhIL-17 in vitro enhance regeneration and stem cell markers (Figure S6C). Similarly, WIHN of *Il-17a/f*$^{-/-}$ mice has no significant difference from WT mice (Figure S6D). These results suggest that bacteria induced skin regeneration through Myd88 signaling is not γδT cells and IL-17A dependent and more likely through IL-1 as detailed above. We next tested how IL-17 affects skin microbiome. We find that the α-diversity of *Il-17a/f*$^{-/-}$ mice is not significantly different from WT mice, but the *Pseudomonas* increase while other bacteria, including *Staphylococcus,* decrease. These data highlight a common and unique sensitivity of *Staphylococcus* commensal levels to host immune disruption. (Figure S6E and S6F).

Commensal Bacteria Promote Healing in Humans

Finally, in a small trial, we sought to clarify whether this bacterial-promoted regenerative phenotype was conserved across species. Because WIHN has not been definitively identified

in humans, and because WIHN and wound closure correlate in another study (Wei et al., 2020) and in our microbiome results (see above), we used wound closure speed as our endpoint in human subjects.

We therefore tested whether bacteria would enhance wound closure speed in humans. In each individual subject with no recent antibiotic history, we performed bilateral identical punch biopsy wounds to subcutaneous fat and instructed the participants to treat one wound with the common over the counter topical antibiotic Neosporin and the second paired control with Vaseline, both under occlusion. The popliteal fossa was chosen as the study site because previous microbiome sequencing has shown that it possesses one of the highest microbial diversity, richness, and evenness among body sites, and its dominant bacteria is *Staphylococcus* (Grice et al., 2009; Grice and Segre, 2011). To our surprise, Neosporin significantly slows wound healing speed (Figure 6A), consistent with studies in mice (Di Domizio et al., 2020). None of the 6 patients developed contact dermatitis to Neosporin (Shahbazian et al., 2012). Taxonomy results show that *Staphylococcus* is the dominant bacteria on control skin, which is significantly reduced after Neosporin treatment (Figure 6B and 6C). By histology, a complete epithelium forms beneath the scar on Vaseline treated skin. In contrast, reepithelialization is incomplete on the Neosporin treated skin as seen by an epithelial tongue that is still migrating towards wound closure (Figure 6D). Immunofluorescence staining shows higher levels of KRT5 and IL-1β in Vaseline treated than in Neosporin treated skin (Figure 6D). As in our mouse findings, the expression of *WNT7B*, *EGFR*, *PCNA,* and *TNF* are significantly lower in the Neosporin treated tissues, and *BMP6* is significantly higher (Figure 6E) (Iglesias-Bartolome et al., 2018; Kim et al., 2019).

We next performed gene expression analysis on Vaseline versus Neosporin treated wounds. Genes associated with wound healing are significantly higher expressed in Vaseline treated skin (Figure 6F). These include keratins *KRT16, KRT6C*; cell proliferation-related genes *CEP55*, *MAPK13*, and *KIF18A*; and inflammation activation-related genes *CCL24*, *Ly6G6C*, and *C10orf99*. However, fibroblast activation genes, such as *FAP,* are significantly higher in Neosporin treated skin (Figure 6F). Unsupervised cluster analysis confirms these findings with clustering of pre-treatment biopsies of healthy skin (unwounded) and post-treatment biopsies of re-epithelialized skin (wounded) that reveals distinct keratin expression landscapes between groups (Figure 6G). Similarly, Neosporin and Vaseline treated samples also separately cluster with the former associated with low expression for most of the wound keratins, skin regeneration related genes, and chemokines (Figure 6G) (Iglesias-Bartolome et al., 2018; Nelson et al., 2015).

Finally, gene enrichment analysis again demonstrates a signature for *S. aureus* infection pathway associating with improved wound healing in the Vaseline treatment group, corroborating our results in mice (Figure 6H). Transcripts for immune activation, skin development, and epidermis development are significantly higher in the Vaseline treated skin (Figure 6I), while collagen related transcripts are significantly higher in the Neosporin treated skin (Figure 6I). These functional results indicate that the reduction of skin resident microbes inhibits both mouse and human healing capacities.

DISCUSSION

Regeneration abilities of species are largely thought to be an intrinsic property. Here we show that the extrinsic microbiome modulates regeneration, with clear clinical implications. Currently, topical antibiotics are in routine use after minor skin trauma by consumers and even some physicians. Additionally, high levels of antibiotics use are a culprit for increasing antibiotic resistance. Our results suggest the benefits of decreased topical antibiotic use. We show that the microbiome improves regeneration in a skin wounding model where de novo neogenic hair follicles form in a morphogenesis event that recapitulates embryonic development. Not only is the microbiome important for this regeneration, but even the addition of pathogenic levels of bacteria enhances the effect. We demonstrate the mechanism is through a signaling cascade where IL-1β and its receptor IL-1R activate Myd88 in keratinocytes. We also show that even in humans, our commensal microbiome is functionally important for wound closure speed. These results highlight the evolved symbiosis between wound healing and commensal bacteria and the deleterious effects of routine topical antibiotic use in humans.

The microbiome is an underappreciated factor that might even commonly confound ongoing laboratory studies on regeneration given differences in animal cage care across institutions. Our results are consistent with an emerging literature on the positive roles of skin and intestinal microbiota, including several that are consistent with a promotion of wound healing by skin microbiota in mouse and human (Kasuya et al., 2018; Nelson et al., 2015; Wang et al., 2017). One outlier study found GF mice heal faster than conventional mice potentially due to differences such as the use of distinct strains, older ages, smaller wounds, and different isolation protocols (Kulkarni et al., 2017). Instead, a very recently published study showed that antibiotics inhibit wound healing in mice, consistent with our findings (Di Domizio et al., 2020). Therefore, there is an emerging consensus where the microbiome promotes wound healing through multiple distinct mechanisms.

Our results are generally in line with infectious disease reports that the IL-1β-IL-1R-MyD88 signal induced by *S. aureus* accelerates the proliferation of keratinocytes and inhibits the differentiation of keratinocyte in lesional skin (Hanel et al., 2016; Nestle et al., 2009). Similarly, our work adds to efforts to understand common inflammatory skin diseases, such as atopic dermatitis, where *S. aureus* is overabundant (Byrd et al., 2017; Ng et al., 2017). For example, our work raises the speculation that lack of scarring seen in patients after the resolution of even severe atopic dermatitis might in part be from *S. aureus* abundance. Our findings also suggest that—despite its potential for pathogenic infection—the prevalence of *Staphylococcus aureus* in even normal appearing healthy skin might be maintained through evolution given its beneficial effects on wound healing, akin to other reports (Kumar et al., 2015), and the positive effects of *S. epidermidis* on skin immune training and wound healing (Constantinides et al., 2019). Our findings also raise important questions regarding microbial governance and stability given how IL-1, My88, or IL-17 loss modify the microbiome composition, especially *Staphylococcus aureus* abundance.

This effort was motived through an analysis of our three previous independent studies that correlated gene signature of high WIHN with that of *S. aureus* infection, but other bacteria

are likely also important for regeneration. Similarly, aside from the innate immune mechanisms studied here, it is an important and fruitful area of future study to test how the adaptive immune system supports regeneration during bacterial stimulation (Kalekar et al., 2019; Wang et al., 2019). Clearly important future work will define more details on IL-1 dependent and independent mechanisms through which the microbiome promotes healing.

In summary, our study demonstrates the positive effects of resident microbes on the healing of human and mouse skin wounds. Future questions will address if there are particular commensal microbes that have a greater effect at positively promoting healing and regeneration. and indeed if there might be negatively oriented ones. Our results demonstrate the importance for discontinuing the common use of topical prophylactic antibiotics.

STAR⊗METHODS

RESOURCE AVAILABILITY

Lead Contact—Further information and requests for reagents and resources should be directed to and will be fulfilled by the Lead Contact, Luis Garza (LAG@jhmi.edu).

Materials availability—This study did not generate new unique reagents.

Data and code availability—The microarray data were deposited in the NCBI Gene Expression Omnibus (GEO) under accession number GSE158613, GSE158614, and GSE158616. The 16S rDNA sequences data were deposited with the NCBI Sequence Read Archive (SRA) under accession number PRJNA665993 and PRJNA665992.

EXPERIMENTAL MODEL AND SUBJECT DETAILS

Animal—All mouse culture and experiments were approved by the Johns Hopkins University Animal Committee and based on IACUC protocol MO17M298 (non-infection experiment) and MO25M421 (infection experiment); mouse strains and corresponding genotyping primers are listed in Mouse strains Table. 21-day-old, 8 to 12-gram male and female mice in their first telogen phase were selected. All mouse backgrounds are based on C57BL/6. GF mouse experiments were conducted in the Germ-Free laboratory of the Johns Hopkins Bloomberg School of Public Health, while SPF mouse experiments were conducted in the Johns Hopkins School of Medicine animal facilities. C57BL/6j, *Tlr2*$^{-/-}$ mice (B6.129-Tlr2tm1Kir/J), *Il-1r*$^{-/-}$ mice (B6.129S7-Il1r1tm1Imx/J), *Myd88*−/− mice (B6.129P2(SJL)-Myd88tm1.1Defr/J), *LysM*-cre mice (B6.129P2-Lyz2tm1(cre)Ifo/J), and *Myd88*$^{fl/fl}$ (B6.129P2(SJL)-Myd88tm1Defr/J) mice were obtained from Jackson Laboratories. *LysM*-cre mice were crossed with *Myd88*$^{fl/fl}$ mice to obtain the *LysM*-cre × *Myd88*$^{fl/fl}$ mouse strain. The *Il-36r*$^{-/-}$ mice (Il1rl2tm1Hblu) were acquired from Amgen, Inc and obtained from Johns Hopkins University School of Medicine through MTA (material transfer agreement). *K14-Il-1r*$^{-/-}$ mice and *K14-Myd88*$^{-/-}$mice were generously provided by Nate Archer (JHMI). *Il-1a*$^{-/-}$ mice, *Il-1β*$^{-/-}$mice and *Il-17a/f*$^{-/-}$ mice were generously provided by Yoichiro Iwakura (University of Tokyo) and obtained from Johns Hopkins University School of Medicine through MTA. DNA was extracted from mouse tails, and transgenes were confirmed via PCR.

Husbandry and housing conditions of experimental animals—Germ-free mice were housed in the germ-free bubble of the Germ-Free laboratory in the Johns Hopkins Bloomberg School of Public Health. SPF mice were housed in the biological safety cabinet of Johns Hopkins School of Medicine. In transfer experiments, GF mice were wounded in the germ-free bubble and then transferred to the Johns Hopkins School of Medicine SPF mice facility immediately and co-house with wounded SPF mice until evaluation of hair follicle regeneration. In cage change experiments, cages were changed in the following frequencies immediately following weaning: one group received 1 new cage per day, and the other group received no changes. Both frequencies were performed for 24 days until the evaluation of hair follicle regeneration. Unless otherwise noted, mice were housed together, with less than five mice per cage.

Culture conditions for in vitro systems—Keratinocytes were cultured with keratinocyte growth medium (KGM-Gold) (Lonza, 00192152) in 37°C, 5% CO2 incubator. Culture media was changed every other day, and all primary keratinocytes were passaged at least once to remove dead and contaminating cells.

Human samples.—Human skin samples were obtained under the terms of informed consent and Hopkins IRB (NA_00033375) following Helsinki principles. Human keratinocytes were isolated from discarded neonatal foreskins and were processed as described previously (Kim et al., 2019). For the clinical trial on wound healing's dependence on the microbiome, 4mm full-thickness skin punch biopsies were obtained from adult popliteal fossae (PF).

Human skin microbiome study.—Under Hopkins IRB (NA_00033375), six adults (3 male, 3 female; 2 Caucasian, 1 Black, 2 Hispanic, 1 Asian) were enrolled from February 21 through December 4, 2020 at the Johns Hopkins Department of Dermatology, Baltimore, Maryland with an average age of 28. Inclusion criteria included all adults, ages 18–53, with normal, healthy skin. Exclusion criteria included the presence of disordered skin or infectious disease, self-reported pregnancy, and failure to provide informed consent. Those with a recent history of topical antibiotics use in the previous 7 days, including antibacterial soaps and/or washes, or systemic antibiotics use in the previous 6 months were also excluded. All study activities were approved and overseen by the Johns Hopkins Institutional Review Board, and all patients provided written and informed consent. No alterations in the standard of care occurred.

METHOD DETAILS

Sample collection.—4-mm punch biopsies, microbiome swabs, and clinical photographs of bilateral PF were obtained from participants under the above IRB protocol. Participants were asked to avoid washing 24 hours prior to sample collection and to use scent-free, non-antibacterial soap for the duration of the study. Samples were collected at two visits spanning an average of 15 days, including at a baseline visit prior to intervention (Day 0) and at a follow-up visit following secondary intention to obtain post-treatment samples (Day 15). A total of 24 skin biopsies and 12 microbiome samples were obtained from 6 individuals at identical anatomical sites across 2 time points. For microbiome collection,

Puritan sterile foam-tipped applicators (Puritan, 25–1506 1PF TT) were premoistened with lysis buffer (20 mmol/L Tris [pH 8.0] (Quality Biological, 723017), 2 mmol/L EDTA (Sigma, E4884), and 1.2% Triton X-100 (sigma, T9284) prior to wounding and vigorously rubbed ~40 times, covering 6cm^2 areas. Control samples followed identical procedures with exposure to air only. For tissue collection, 1% lidocaine with epinephrine was administered, and 4mm full-thickness punch biopsies were obtained from the center of swabbed PF. For the left PF of patient#1 to patient #3 and the right PF of patient#4 to patient #6, the wound was washed with Hibiclens (Molnlycke, 57516), and Neosporin was applied (Johnson & Johnson); for the right PF of patient#1 to patient #3 and the left PF of patient#4 to patient #6, Vaseline (Unilever) was applied. Both sites were occluded with bandages, and participants were asked to rebandage PF daily with Neosporin and Vaseline, respectively, until Day 15 to evaluate the changes in microbiome and gene expressions. Written and verbal instructions were provided. Day 0 and Day 15 photographs of wound size were quantified by ImageJ to calculate healing speed, and tissue and microbiome samples were processed for analysis.

16S rDNA extraction, PCR amplification, and sequencing.—Microbiome samples from human skin were sent to CosmoID, Rockville, Maryland. Microbiome samples from mouse skin were sent to University of Michigan Medical School, Microbial Systems Molecular Biology Laboratory for Illumina 16S rDNA gene sequencing. In general, DNA was lysed by mechanical magnetic bead impacting and isolated by magnetic technology. The DNA was used to generate 16s rDNA libraries, which has been described previously(Seekatz et al., 2015). The barcoded dual-index sequencing primers targeting to the 16sRNA V4 region amplify the DNA(Kozich et al., 2013). After PCR reactions, pooled amplicon library was then sequenced on the Illumina MiSeq platform using the 500 cycle MiSeq V2 Reagent kit (catalog no. MS-102–2003) according to the manufacturer's instructions with modifications of the primer set with custom read 1/read 2 and index primers added to the reagent cartridge. The "Preparing Libraries for Sequencing on the MiSeq" (part 15039740, Rev. D) protocol was used to prepare libraries with a final load concentration of 5.5 pM, spiked with 15% PhiX to create diversity within the run. Fastq files were generated when the 2 × 250 bp sequencing completed.

16s rDNA sequence analysis pipeline and bioinformatics analysis.—The consensus sequences from each of these paired ends were obtained using Fast Length Adjustment of SHort reads (FLASH_v1.2.11). The following parameters were used: max-overlap =250. Fastx_toolkit_v0.0.14 was used to convert fastq to fasta. The consensus fasta sequences were then clustered using the program AbundantOTU_v0.93. This program clustered these sequences into Operational Taxonomic Units (OTUs) with an average percent identity of 97%. The software also generated a consensus sequence for each OTU. To check for chimeras, consensus sequences for each OTU were fed into usearch_v8.1. The found chimeric sequences were removed and default parameters were used. Based Taxonomic Classification Method (BLCA) and "GreenGenes_v13.5" were used for taxonomic classification. OTU and Shannon levels were generated by QIIME 2's diversity analyses through the q2-diversity plugin, which supported computing α- and β-diversity metrics (Bolyen et al., 2019). The PCA (principal component analysis) of the β-diversity was based

on R package stats cmdscale function. Taxonomic analysis α- and β-diversity was visualized by R package ggplot2.

Wound-induced hair neogenesis (WIHN) model.—All animal experiments followed our previous WIHN model protocol (Kim et al., 2019; Nelson et al., 2015). Mice were anesthetized with vaporizing anesthesia (Baxter, Isoflurane), shaved, and denuded of 1.44 cm^2 full thickness skin using sterile procedures. On WD24, the number of regenerative hair follicles in mice were visualized and quantified using reflectance confocal scanning laser microscopy (CSLM) as described before(Kim et al., 2019; Nelson et al., 2015). Germ-free operations were performed in the germ-free bubble of the Germ-Free laboratory in the Johns Hopkins Bloomberg School of Public Health. SPF operations were performed in the biological safety cabinet of Johns Hopkins School of Medicine. In Vaseline and Neosporin experiments, both groups of mice were treated with 500mg Vaseline and Neosporin topical applications one day before wounding and around the wound until healed. For exogenous bacteria challenge, 1e4 ~1e8 /100ul *P. aeruginosa*, *S. pyogenes, S. aureus*, *S. xylosus*, and *S. epidermidis* (see detail in supplemental figures) were injected under the scab on WD3. 1e7/100ul *S. aureus* and *S. epidermidis* were used for WT mice experiments and 1e6/100ul *S. aureus* were used for all other mouse strains experiments without indicated dosage. Wound beds were photographed from WD1 to WD17, and wound size was quantified by ImageJ. 1e7/100ul Heat-kill *S. aureus*, 500ng/100ul rmIL-1a (R&D systems), and 500ng/100ul rmIL-1β (R&D systems) were injected under the scab on WD3 as well. PBS was administered as a control (vehicle). Cohousing occurred for mice of identical treatments, same gene knockouts, and microbiome transfer experiments. Single-caged mice were used to study the influence of inflammatory signals on epidermal microbiome.

Human and mouse keratinocytes isolation.—Human keratinocytes were obtained from discarded neo-natal foreskins as previously described (Kim et al., 2019). Mouse keratinocytes were obtained from euthanized newborn mouse skin and were processed following the same protocol as human keratinocytes. In short, skin was cut and washed by 70% ethanol (Pharmco, 111000200) and Phosphate-Buffered Saline (PBS) (Gibco, 10010–023). Skin was digested in 0.4% dispase II (Sigma, D4693) at 4°C overnight. After next-day separation from the dermis, the epidermis was sectioned and digested by 0.025% trypsin/EDTA (Lonza, CC-5012.) at 37°C for 15 m. Trypsin Neutralization Solution (TNS) (Lonza, CC-5002) was added to stop the digestion. After filtration with 40um filter and centrifugation at 2000rpm for 5 m, keratinocytes were resuspended with keratinocyte growth medium (KGM-Gold) (Lonza, 00192152).

Bacteria strains, preparation and bioluminescent imaging (BLI).—As described before(Archer et al., 2019; Liu et al., 2017), the bioluminescent *Staphylococcus aureus*: NRS384, *Staphylococcus epidermidis*: Xen43, *Staphylococcus xylosus*: NKA352, *Streptococcus pyogenes*: Xen20 and *Pseudomonas aeruginosa*: Xen41 were used in all experiments. For bacterial preparation, *S. aureus* and *S. epidermidis* were streaked on the tryptic soy agar (TSA) plate. After incubation at 37 °C overnight, single luminescent colonies were picked from the plate and cultured into tryptic soy broth (TSB (BD Bacto, 8330706)) and shaken at 37°C, 240rpm for 18 hours, following by 1:50 dilution to new TSB

for 3 hours to reach the mid-logarithmic (ME) phase. After centrifugation, washing and resuspension, *S. aureus* and *S. epidermidis* were finally resuspended in sterile PBS at the required concentration. *S. pyogenes* was streaked onto a pre-warm TSA plate. After incubation at 37°C overnight, single luminescent colonies were picked from the plate and cultured into pre-warm Todd-Hewitt broth (Acumedia, 741–60647), supplemented with 0.5% yeast extract (Sigma, 70161–100G) (THY)) in sterile, sealed tubes. Bacteria was incubated at 37°C for 24 h without shaking. Culture media was inverted 5–10 times and diluted 1:50 to new THY at 37°C for 4 h without shaking to reach the ME phase. After centrifugation, washing and resuspension by PBS, the *S. pyogenes* was finally resuspended in sterile PBS at the required concentration. *P. aeruginosa* was streaked on Luria broth (LB (BD Difco, 244620)) agar plates. After incubation at 37°C overnight, single luminescent colonies were picked from the plate and cultured into LB and shaken at 37°C, 240rpm for 18 h, followed by 1:50 dilution to new LB for 3 h to reach the ME phase. The bacteria were planted on TSA or LB agar plates overnight for measuring the number of CFU, which was determined by absorbance (A600). Lumina III IVIS (PerkinElmer) was used for bioluminescent imaging of anesthetized mice, and the signal intensity total flux (p/s) was measured by Living Image software (PerkinElmer).

Histology, Immunofluorescence and fluorescence microscopy.—Human and mouse skin were flattened and fixed by 4% paraformaldehyde (PFA (Thermo Scientific, J19943-K2)). After fixation for 48 h, biopsies were submitted to Johns Hopkins Oncology Tissue Services Core. Briefly, biopsies were embedded in paraffin and sliced into 4um thicknesses. Biopsy sections were mounted onto slides and stained by hematoxylin and eosin (H&E). Biopsies sections were de-paraffinized before using Target Retrieval Solution for antigen retrieval. After washing and permeabilization by Tris-buffered saline (Quality Biological, 351–086-101), 0.1% Tween 20(Sigma, P2287) (TBST) buffer, sections were blocked by 5% sheep serum and 1% Bovine Serum Albumin (BSA (Fisher Bioreagents, BP9703–100)) at room temperature for 1h. Sections were then incubated by the primary antibody (Antibodies for Immunostaining Table) dissolved in Antibody Diluent (Agilent Dako, S0809) overnight at 4°C. After washing by TBST, sections were incubated by fluorescent binding secondary antibodies at room temperature for 1h. Following finial washing, cell nuclei were stained by DAPI, and sections were mounted with mounting medium. All slides were imaged using DFC365FX (Leica), and ImageJ was used for quantitative analysis of fluorescence intensity. The fold change is the standardization of the signal expression at the wound bed epidermis to the adjacent normal skin. Oil red O staining was performed on 15 um frozen section using Oil Red O kit (abcam, ab150678) and its commercial protocol.

RNA Isolation and Quantitative real-time PCR.—For human in vivo/in vitro and for mouse in vivo samples, total RNA was isolated after homogenization when applicable using RNeasy Mini Kit (Qiagen, 74106). RNA concentration and purity was calculated by NanoDrop2000c (Thermo Fisher Scientific). RNA was reverse transcribed into cDNA by using High-Capacity cDNA Reverse Transcription Kit (Applied Biosystems, 4368813). Taqman probes with FAM dye, listed in Oligonucleotides Table were used to detect the expression of the interested target genes. RPLP0 and β-actin were used as housekeeping

genes for humans and mice separately and detected by Taqman probes with VIC dye. Target genes' relative expression were calculated by ΔΔCT method.

T cell isolation.—The single-cell lymphatic suspension is obtained by pushing the wounded WT and Myd88−/− skin secondary lymph nodes through the 40um filter to remove impurities and use FACS buffer to drain the cells. CD3 + T cells are obtained by using mouse Pan T cell isolation kit (Miltenyi Biotec, 130095130). Using negative selection, CD11b, CD11c, CD45R, CD19, CD49b, CD105, MHCII and Ter-119 positive cells were adsorbed on the magnetic column. The remaining T cells were collected by flowing the magnetic column.

Flow cytometry.—The single cell suspension from the skin was digested by RPMI (Gibco, 11875–093) with Liberase (Roche, 05401020001) and 10% DNase at 37°C for 1h. The suspension was filtered through a 40um cell filter to remove tissue debris following by resuspension in FACS buffer. After washing by FACS buffer, cells were stained with Viability Fixable Dye (Miltenyi Biotec) and surface markers antibody. Neutrophil, monocyte, macrophage, M2macrophage, CD4+T, and γδT cells were stained by antibodies against CD11b, Ly6C, Ly6G, F4/80, CD206, CD3, γδTCR (Antibodies for Flow cytometry Table) for 30m at 4°C. Following subsequent washing, MACSQuant flow cytometer (Miltenyi Biotec) was used for cells detection, and FlowJo software (Treestar) was used for data analysis.

Tensile strength measurements—The tensile strength of mouse skin was measured using a ZP-100N digital force gauge (Baoshishan, China). Before testing, mouse skin was dissected and cut into strips approximately 15 mm × 5mm. Each skin sample was then mounted onto the force gauge by securing its two ends using a pair of clamps. One clamp was mechanically coupled to the force gauge, while the other clamp was fixed at the immobile test stand made of steel frames. To avoid tissue damage and slipping, the clamps were wrapped with a layer of PBS-dampened gauze. Clamps and skin sample were carefully aligned before each test to ensure uniaxial stretching. To test the tensile strength of the skin sample, the sample was stretched by moving the force gauge along the rail of the test stand, increasing the distance between the two clamps. The skin sample was stretched at the rate of ~2 mm/s. The incremental force magnitudes required for elongation of sample were recorded by the digital force gauge until failure. Failure was defined as the data point when the force magnitude measured by the gauge started to drop. The peak force recorded during each test immediately before sample failure was reported as the tensile strength of that sample.

QUANTIFICATION AND STATISTICAL ANALAYSIS

Microarray, RNA-seq and proteomic analysis.—Total RNA from early wound bed skin of GF, SPF, *Rara*$^{-/-}$, WT, *S. aureus* treated, and PBS treated mice was submitted to the JHMI Transcriptomics and Deep Sequencing Core; human PF skin from the clinical trial was submitted, too. The 1.0ST exon sequencing of human and mouse RNA was performed according to the manufacturer's standard protocol. The raw affymetrix CEL data was standardized using Robust Multichip Analysis (RMA) algorithm for comparison. The results

of Microarray from *Rnase1*$^{-/-}$ and WT mice are as described before. Total RNA from T cells of *Myd88*$^{-/-}$ and WT mice was sequenced by Beijing Genomics Institute. After quality control, the samples were sequenced on DNBseq platform following manufactory strand-specific library preparation. HISAT2 was used to map reference genome. Genic read counts were finally normalized to FPKM for comparison. Proteins from the wound center and wound edges were analyzed by proteomics. In short, as previously described(Kim et al., 2019), we used Orbitrap Fusion Tribrid mass spectrometer (Thermo Scientific) for protein profiling and obtained the protein expression level by MS Amanda algorithm. Standard bioinformatics procedures were performed, including standardization of gene expression, definition of differentially expressed genes, and GO and KEGG enrichment analysis. We used the R package *limma*(Ritchie et al., 2015) to define DEGs among different groups. We performed the *clusterProfiler* R package (Yu et al., 2012) for gene-annotation enrichment analysis. The visualization of these results is achieved through the R package ggplots2. The value of immune cells infiltration of S. aureus treated and control mice were analyzed by ImmuCC as described before (Chen et al., 2018).

Statistics

R was used for all statistical analyses. Statistical significance between two groups was analyzed by Student *t-test*. For multiple-group comparisons, one-way ANOVA was used as a parametric method. Data were presented in the form of mean and ± standard error. *P*-value of less than 0.05 was considered statistically significant.

Supplementary Material

Refer to Web version on PubMed Central for supplementary material.

Acknowledgments:

The authors thank the Cutaneous Translational Research Program (CTReP) at the Department of Dermatology for organizing human subjects and preparing tissue samples. Research reported in this publication was supported by the National Institute of Arthritis and Musculoskeletal and Skin Diseases, part of the National Institutes of Health, under R01AR074846 01 to LAG. This work was also supported by the Northrop Grumman Electronic Systems as well as the Thomas Provost, MD Young Faculty Development Fund of Johns Hopkins Dermatology to LAG.

Declaration of interests: L.S.M. is a full-time employee of Janssen Pharmaceuticals and may hold Johnson & Johnson stock and stock options. L.S.M. performed all work at his prior affiliation at Johns Hopkins University School of Medicine, and he has received prior grant support from AstraZeneca, Pfizer, Boehringer Ingelheim, Regeneron Pharmaceuticals, and Moderna Therapeutics; he was also a paid consultant for Armirall and Janssen Research and Development, was on the scientific advisory board of Integrated Biotherapeutics, and is a shareholder of Noveome Biotherapeutics, which are all developing therapeutics against infections (including *S. aureus* and other pathogens) and/or inflammatory conditions.

References

Abo H, Chassaing B, Harusato A, Quiros M, Brazil JC, Ngo VL, Viennois E, Merlin D, Gewirtz AT, Nusrat A, et al. (2020). Erythroid differentiation regulator-1 induced by microbiota in early life drives intestinal stem cell proliferation and regeneration. Nat Commun 11, 513. [PubMed: 31980634]

Archer NK, Jo JH, Lee SK, Kim D, Smith B, Ortines RV, Wang Y, Marchitto MC, Ravipati A, Cai SS, et al. (2019). Injury, dysbiosis, and filaggrin deficiency drive skin inflammation through keratinocyte IL-1alpha release. J Allergy Clin Immunol 143, 1426–1443 e1426. [PubMed: 30240702]

Bolyen E, Rideout JR, Dillon MR, Bokulich NA, Abnet CC, Al-Ghalith GA, Alexander H, Alm EJ, Arumugam M, Asnicar F, et al. (2019). Reproducible, interactive, scalable and extensible microbiome data science using QIIME 2. Nat Biotechnol 37, 852–857. [PubMed: 31341288]

Byrd AL, Deming C, Cassidy SKB, Harrison OJ, Ng WI, Conlan S, Program NCS, Belkaid Y, Segre JA, and Kong HH (2017). Staphylococcus aureus and Staphylococcus epidermidis strain diversity underlying pediatric atopic dermatitis. Sci Transl Med 9.

Cai Y, Xue F, Quan C, Qu M, Liu N, Zhang Y, Fleming C, Hu X, Zhang HG, Weichselbaum R, et al. (2019). A Critical Role of the IL-1beta-IL-1R Signaling Pathway in Skin Inflammation and Psoriasis Pathogenesis. J Invest Dermatol 139, 146–156. [PubMed: 30120937]

Chen Z, Quan L, Huang A, Zhao Q, Yuan Y, Yuan X, Shen Q, Shang J, Ben Y, Qin FX, et al. (2018). seq-ImmuCC: Cell-Centric View of Tissue Transcriptome Measuring Cellular Compositions of Immune Microenvironment From Mouse RNA-Seq Data. Front Immunol 9, 1286. [PubMed: 29922297]

Chu SY, Chou CH, Huang HD, Yen MH, Hong HC, Chao PH, Wang YH, Chen PY, Nian SX, Chen YR, et al. (2019). Mechanical stretch induces hair regeneration through the alternative activation of macrophages. Nat Commun 10, 1524. [PubMed: 30944305]

Constantinides MG, Link VM, Tamoutounour S, Wong AC, Perez-Chaparro PJ, Han SJ, Chen YE, Li K, Farhat S, Weckel A, et al. (2019). MAIT cells are imprinted by the microbiota in early life and promote tissue repair. Science (New York, NY) 366.

Di Domizio J, Belkhodja C, Chenuet P, Fries A, Murray T, Mondejar PM, Demaria O, Conrad C, Homey B, Werner S, et al. (2020). The commensal skin microbiota triggers type I IFN-dependent innate repair responses in injured skin. Nat Immunol 21, 1034–1045. [PubMed: 32661363]

Ekman AK, Bivik Eding C, Rundquist I, and Enerback C (2019). IL-17 and IL-22 Promote Keratinocyte Stemness in the Germinative Compartment in Psoriasis. J Invest Dermatol 139, 1564–1573 e1568. [PubMed: 30684548]

Gay D, Ghinatti G, Guerrero-Juarez CF, Ferrer RA, Ferri F, Lim CH, Murakami S, Gault N, Barroca V, Rombeau I, et al. (2020). Phagocytosis of Wnt inhibitor SFRP4 by late wound macrophages drives chronic Wnt activity for fibrotic skin healing. Sci Adv 6, eaay3704. [PubMed: 32219160]

Gay D, Kwon O, Zhang Z, Spata M, Plikus MV, Holler PD, Ito M, Yang Z, Treffeisen E, Kim CD, et al. (2013). Fgf9 from dermal gammadelta T cells induces hair follicle neogenesis after wounding. Nat Med 19, 916–923. [PubMed: 23727932]

Godwin JW, Pinto AR, and Rosenthal NA (2013). Macrophages are required for adult salamander limb regeneration. Proc Natl Acad Sci U S A 110, 9415–9420. [PubMed: 23690624]

Grice EA, Kong HH, Conlan S, Deming CB, Davis J, Young AC, Program NCS, Bouffard GG, Blakesley RW, Murray PR, et al. (2009). Topographical and temporal diversity of the human skin microbiome. Science (New York, NY) 324, 1190–1192.

Grice EA, and Segre JA (2011). The skin microbiome. Nat Rev Microbiol 9, 244–253. [PubMed: 21407241]

Hanel KH, Pfaff CM, Cornelissen C, Amann PM, Marquardt Y, Czaja K, Kim A, Luscher B, and Baron JM (2016). Control of the Physical and Antimicrobial Skin Barrier by an IL-31-IL-1 Signaling Network. J Immunol 196, 3233–3244. [PubMed: 26944931]

Hendley JO, and Ashe KM (2003). Eradication of resident bacteria of normal human skin by antimicrobial ointment. Antimicrob Agents Chemother 47, 1988–1990. [PubMed: 12760881]

Huang X, Feng Z, Jiang Y, Li J, Xiang Q, Guo S, Yang C, Fei L, Guo G, Zheng L, et al. (2019). VSIG4 mediates transcriptional inhibition of Nlrp3 and Il-1beta in macrophages. Sci Adv 5, eaau7426. [PubMed: 30662948]

Iglesias-Bartolome R, Uchiyama A, Molinolo AA, Abusleme L, Brooks SR, Callejas-Valera JL, Edwards D, Doci C, Asselin-Labat ML, Onaitis MW, et al. (2018). Transcriptional signature primes human oral mucosa for rapid wound healing. Sci Transl Med 10.

Ishida Y, Kuninaka Y, Yamamoto Y, Nosaka M, Kimura A, Furukawa F, Mukaida N, and Kondo T (2020). Pivotal Involvement of the CX3CL1-CX3CR1 Axis for the Recruitment of M2 Tumor-Associated Macrophages in Skin Carcinogenesis. J Invest Dermatol 140, 1951–1961 e1956. [PubMed: 32179066]

Ito M, Liu Y, Yang Z, Nguyen J, Liang F, Morris RJ, and Cotsarelis G (2005). Stem cells in the hair follicle bulge contribute to wound repair but not to homeostasis of the epidermis. Nat Med 11, 1351–1354. [PubMed: 16288281]

Ito M, Yang Z, Andl T, Cui C, Kim N, Millar SE, and Cotsarelis G (2007). Wnt-dependent de novo hair follicle regeneration in adult mouse skin after wounding. Nature 447, 316–320. [PubMed: 17507982]

Joost S, Jacob T, Sun X, Annusver K, La Manno G, Sur I, and Kasper M (2018). Single-Cell Transcriptomics of Traced Epidermal and Hair Follicle Stem Cells Reveals Rapid Adaptations during Wound Healing. Cell Rep 25, 585–597 e587. [PubMed: 30332640]

Kalekar LA, Cohen JN, Prevel N, Sandoval PM, Mathur AN, Moreau JM, Lowe MM, Nosbaum A, Wolters PJ, Haemel A, et al. (2019). Regulatory T cells in skin are uniquely poised to suppress profibrotic immune responses. Science immunology 4, eaaw2910. [PubMed: 31492709]

Kasuya A, Ito T, and Tokura Y (2018). M2 macrophages promote wound-induced hair neogenesis. J Dermatol Sci 91, 250–255. [PubMed: 29776717]

Kathju S, Gallo PH, and Satish L (2012). Scarless integumentary wound healing in the mammalian fetus: molecular basis and therapeutic implications. Birth Defects Res C Embryo Today 96, 223–236. [PubMed: 23109318]

Kim D, Chen R, Sheu M, Kim N, Kim S, Islam N, Wier EM, Wang G, Li A, Park A, et al. (2019). Noncoding dsRNA induces retinoic acid synthesis to stimulate hair follicle regeneration via TLR3. Nat Commun 10, 2811. [PubMed: 31243280]

Kozich JJ, Westcott SL, Baxter NT, Highlander SK, and Schloss PD (2013). Development of a dual-index sequencing strategy and curation pipeline for analyzing amplicon sequence data on the MiSeq Illumina sequencing platform. Appl Environ Microbiol 79, 5112–5120. [PubMed: 23793624]

Kulkarni NN, Adase CA, Zhang LJ, Borkowski AW, Li F, Sanford JA, Coleman DJ, Aguilera C, Indra AK, and Gallo RL (2017). IL-1 Receptor-Knockout Mice Develop Epidermal Cysts and Show an Altered Innate Immune Response after Exposure to UVB Radiation. J Invest Dermatol 137, 2417–2426. [PubMed: 28754339]

Kumar P, Kretzschmar B, Herold S, Nau R, Kreutzfeldt M, Schutze S, Bahr M, and Hein K (2015). Beneficial effect of chronic Staphylococcus aureus infection in a model of multiple sclerosis is mediated through the secretion of extracellular adherence protein. J Neuroinflammation 12, 22. [PubMed: 25644616]

Kyritsis N, Kizil C, Zocher S, Kroehne V, Kaslin J, Freudenreich D, Iltzsche A, and Brand M (2012). Acute inflammation initiates the regenerative response in the adult zebrafish brain. Science (New York, NY) 338, 1353–1356.

Lai Y, Di Nardo A, Nakatsuji T, Leichtle A, Yang Y, Cogen AL, Wu ZR, Hooper LV, Schmidt RR, von Aulock S, et al. (2009). Commensal bacteria regulate Toll-like receptor 3-dependent inflammation after skin injury. Nat Med 15, 1377–1382. [PubMed: 19966777]

Larson BJ, Longaker MT, and Lorenz HP (2010). Scarless fetal wound healing: a basic science review. Plast Reconstr Surg 126, 1172–1180. [PubMed: 20885241]

Lee P, Gund R, Dutta A, Pincha N, Rana I, Ghosh S, Witherden D, Kandyba E, MacLeod A, Kobielak K, et al. (2017). Stimulation of hair follicle stem cell proliferation through an IL-1 dependent activation of gammadeltaT-cells. Elife 6.

Liao W, Hei TK, and Cheng SK (2017). Radiation-Induced Dermatitis is Mediated by IL17-Expressing gammadelta T Cells. Radiat Res.

Lim CH, Sun Q, Ratti K, Lee SH, Zheng Y, Takeo M, Lee W, Rabbani P, Plikus MV, Cain JE, et al. (2018). Hedgehog stimulates hair follicle neogenesis by creating inductive dermis during murine skin wound healing. Nat Commun 9, 4903. [PubMed: 30464171]

Liu H, Archer NK, Dillen CA, Wang Y, Ashbaugh AG, Ortines RV, Kao T, Lee SK, Cai SS, Miller RJ, et al. (2017). Staphylococcus aureus Epicutaneous Exposure Drives Skin Inflammation via IL-36-Mediated T Cell Responses. Cell host & microbe 22, 653–666 e655. [PubMed: 29120743]

Miller LS, O'Connell RM, Gutierrez MA, Pietras EM, Shahangian A, Gross CE, Thirumala A, Cheung AL, Cheng G, and Modlin RL (2006). MyD88 mediates neutrophil recruitment initiated by IL-1R

but not TLR2 activation in immunity against Staphylococcus aureus. Immunity 24, 79–91. [PubMed: 16413925]

Nelson AM, Loy DE, Lawson JA, Katseff AS, Fitzgerald GA, and Garza LA (2013). Prostaglandin D2 inhibits wound-induced hair follicle neogenesis through the receptor, Gpr44. J Invest Dermatol 133, 881–889. [PubMed: 23190891]

Nelson AM, Reddy SK, Ratliff TS, Hossain MZ, Katseff AS, Zhu AS, Chang E, Resnik SR, Page C, Kim D, et al. (2015). dsRNA Released by Tissue Damage Activates TLR3 to Drive Skin Regeneration. Cell Stem Cell 17, 139–151. [PubMed: 26253200]

Nestle FO, Kaplan DH, and Barker J (2009). Psoriasis. N Engl J Med 361, 496–509. [PubMed: 19641206]

Ng CY, Huang YH, Chu CF, Wu TC, and Liu SH (2017). Risks for Staphylococcus aureus colonization in patients with psoriasis: a systematic review and meta-analysis. Br J Dermatol 177, 967–977. [PubMed: 28160277]

Park S, Gonzalez DG, Guirao B, Boucher JD, Cockburn K, Marsh ED, Mesa KR, Brown S, Rompolas P, Haberman AM, et al. (2017). Tissue-scale coordination of cellular behaviour promotes epidermal wound repair in live mice. Nat Cell Biol 19, 155–163. [PubMed: 28248302]

Plikus MV, Guerrero-Juarez CF, Ito M, Li YR, Dedhia PH, Zheng Y, Shao M, Gay DL, Ramos R, Hsi TC, et al. (2017). Regeneration of fat cells from myofibroblasts during wound healing. Science (New York, NY) 355, 748–752.

Qi C, Xu L, Deng Y, Wang G, Wang Z, and Wang L (2018). Sericin hydrogels promote skin wound healing with effective regeneration of hair follicles and sebaceous glands after complete loss of epidermis and dermis. Biomater Sci 6, 2859–2870. [PubMed: 30259043]

Ritchie ME, Smyth GK, Phipson B, Wu D, Hu Y, Shi W, and Law CW (2015). limma powers differential expression analyses for RNA-sequencing and microarray studies. Nucleic Acids Research 43, e47–e47. [PubMed: 25605792]

Salgado RM, Alcantara L, Mendoza-Rodriguez CA, Cerbon M, Hidalgo-Gonzalez C, Mercadillo P, Moreno LM, Alvarez-Jimenez R, and Krotzsch E (2012). Post-burn hypertrophic scars are characterized by high levels of IL-1beta mRNA and protein and TNF-alpha type I receptors. Burns 38, 668–676. [PubMed: 22226222]

SanMiguel AJ, Meisel JS, Horwinski J, Zheng Q, and Grice EA (2017). Topical Antimicrobial Treatments Can Elicit Shifts to Resident Skin Bacterial Communities and Reduce Colonization by Staphylococcus aureus Competitors. Antimicrob Agents Chemother 61.

Scharschmidt TC, Vasquez KS, Pauli ML, Leitner EG, Chu K, Truong HA, Lowe MM, Sanchez Rodriguez R, Ali N, Laszik ZG, et al. (2017). Commensal Microbes and Hair Follicle Morphogenesis Coordinately Drive Treg Migration into Neonatal Skin. Cell host & microbe 21, 467–477 e465. [PubMed: 28343820]

Seekatz AM, Theriot CM, Molloy CT, Wozniak KL, Bergin IL, and Young VB (2015). Fecal Microbiota Transplantation Eliminates Clostridium difficile in a Murine Model of Relapsing Disease. Infect Immun 83, 3838–3846. [PubMed: 26169276]

Shahbazian JH, Hartzell TL, Pandey AK, and Azari KK (2012). Allergic dermatitis due to topical antibiotics. West J Emerg Med 13, 380–382. [PubMed: 22942939]

Taniguchi K, Wu LW, Grivennikov SI, de Jong PR, Lian I, Yu FX, Wang K, Ho SB, Boland BS, Chang JT, et al. (2015). A gp130-Src-YAP module links inflammation to epithelial regeneration. Nature 519, 57–62. [PubMed: 25731159]

Villano JS, Rong F, and Cooper TK (2014). Bacterial infections in Myd88-deficient mice. Comp Med 64, 110–114. [PubMed: 24674585]

Walport MJ (2001). Complement. First of two parts. N Engl J Med 344, 1058–1066. [PubMed: 11287977]

Wang ECE, Dai Z, Ferrante AW, Drake CG, and Christiano AM (2019). A Subset of TREM2(+) Dermal Macrophages Secretes Oncostatin M to Maintain Hair Follicle Stem Cell Quiescence and Inhibit Hair Growth. Cell Stem Cell 24, 654–669 e656. [PubMed: 30930146]

Wang X, Chen H, Tian R, Zhang Y, Drutskaya MS, Wang C, Ge J, Fan Z, Kong D, Wang X, et al. (2017). Macrophages induce AKT/beta-catenin-dependent Lgr5(+) stem cell activation and hair follicle regeneration through TNF. Nat Commun 8, 14091. [PubMed: 28345588]

Wei JJ, Kim HS, Spencer CA, Brennan-Crispi D, Zheng Y, Johnson NM, Rosenbach M, Miller C, Leung DH, Cotsarelis G, et al. (2020). Activation of TRPA1 nociceptor promotes systemic adult mammalian skin regeneration. Sci Immunol 5.

Wu H, Xie S, Miao J, Li Y, Wang Z, Wang M, and Yu Q (2020). Lactobacillus reuteri maintains intestinal epithelial regeneration and repairs damaged intestinal mucosa. Gut Microbes, 1–18.

Wulff BC, Parent AE, Meleski MA, DiPietro LA, Schrementi ME, and Wilgus TA (2012). Mast cells contribute to scar formation during fetal wound healing. J Invest Dermatol 132, 458–465. [PubMed: 21993557]

Yu G, Wang L-G, Han Y, and He Q-Y (2012). clusterProfiler: an R package for comparing biological themes among gene clusters. Omics : a journal of integrative biology 16, 284–287. [PubMed: 22455463]

Zhang Y, Zoltan M, Riquelme E, Xu H, Sahin I, Castro-Pando S, Montiel MF, Chang K, Jiang Z, Ling J, et al. (2018). Immune Cell Production of Interleukin 17 Induces Stem Cell Features of Pancreatic Intraepithelial Neoplasia Cells. Gastroenterology 155, 210–223 e213. [PubMed: 29604293]

Zhou R, Wang G, Kim D, Kim S, Islam N, Chen R, Wang Z, Li A, McCarthy EF, Li L, et al. (2019). dsRNA Sensing Induces Loss of Cell Identity. J Invest Dermatol 139, 91–99. [PubMed: 30120933]

Highlights:

Germ free mice have low skin regeneration.

Skin commensal microbiome and even pathological *S. aureus* induce regeneration.

Bacteria induce regeneration through IL1 β-keratinocyte dependent IL1R/Myd88 signaling.

Commensal bacteria promote healing in humans.

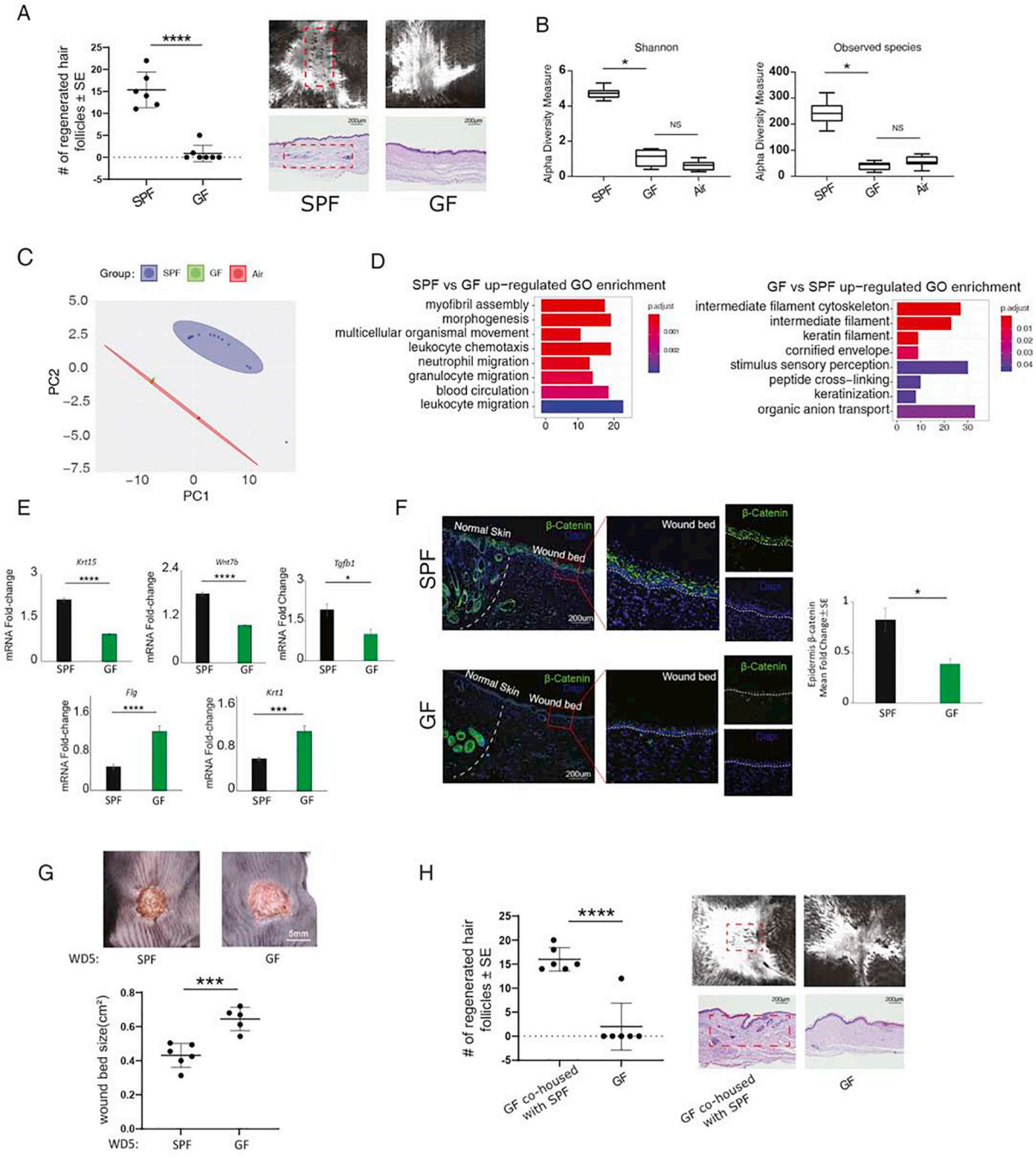

Figure 1. Germ-free (GF) mice have significantly lower wound induced hair follicle neogenesis (WIHN) than Specific pathogen-free (SPF) mice.

(A) GF mice exhibit significantly less WIHN than SPF mice as detected by Confocal Scanning Laser Microscopy (CLSM) (right top), hematoxylin and eosin (H&E) staining (right bottom), and quantification (left). The red dotted line frames the regenerative hair follicles. (n=6–7 independent animals per group). **(B)** Microbiota α-diversity based on the Shannon and Observed species of GF mice were significantly lower than SPF mice and roughly equivalent to air control. (n=4–14 independent animals per group). **(C)** Principal

component analysis (PCA) clustering based on Microbiota β-diversity shows clustering of GF mice with air controls and separation from SPF mice. (n=4–14 independent animals per group). **(D)** Morphogenesis and differentiation categories are included in Gene ontology (GO) enrichment analysis of the top and bottom 500 differentially expressed genes between SPF and GF mice near wound day (WD) 12 wound beds, the day of scab detachment (SD0). (n=3 independent animals per group). **(E)** mRNA expression of stem cell marker (*Krt15*), hair regeneration marker (*Wnt7b, tgfb1*) are higher in SPF mice, while keratinocyte differentiation markers (*Flg, Krt1*) are higher in GF mice. (n=3 independent animals per group). **(F)** β-Catenin expression of SD0 wound bed epidermis as normalized to adjacent normal skin were higher in SPF mice than in GF mice as detected by immunofluorescence staining (up) and quantification (down). The dotted white line demarcates the boundary between the wound bed and normal tissue, and the white scale bar is 200um. (n=3 independent animals per group). **(G)** The wound size of GF mice was significantly bigger than the SPF mice at WD5 as per photos (top) and quantification (bottom) (n=5–6 independent mice per group). **(H)** WIHN is elevated in GF mice after co-housing with SPF mice as detected by CLSM (right top), H&E staining (right bottom), and quantification (left). (n=6 independent animals per group). Representative data from 2~3 independent experiments are shown. Boxplot graphs indicated the value of minimum, first quartile, median, third quartile, and maximum. Scatter plots and histogram graphs indicated means ± SEM; Paired Student *t-test* was used to compare statistical difference, $*P < 0.05$, $**P < 0.01$, $***P < 0.001$, and $****P < 0.0001$. “NS” indicates no significant difference.

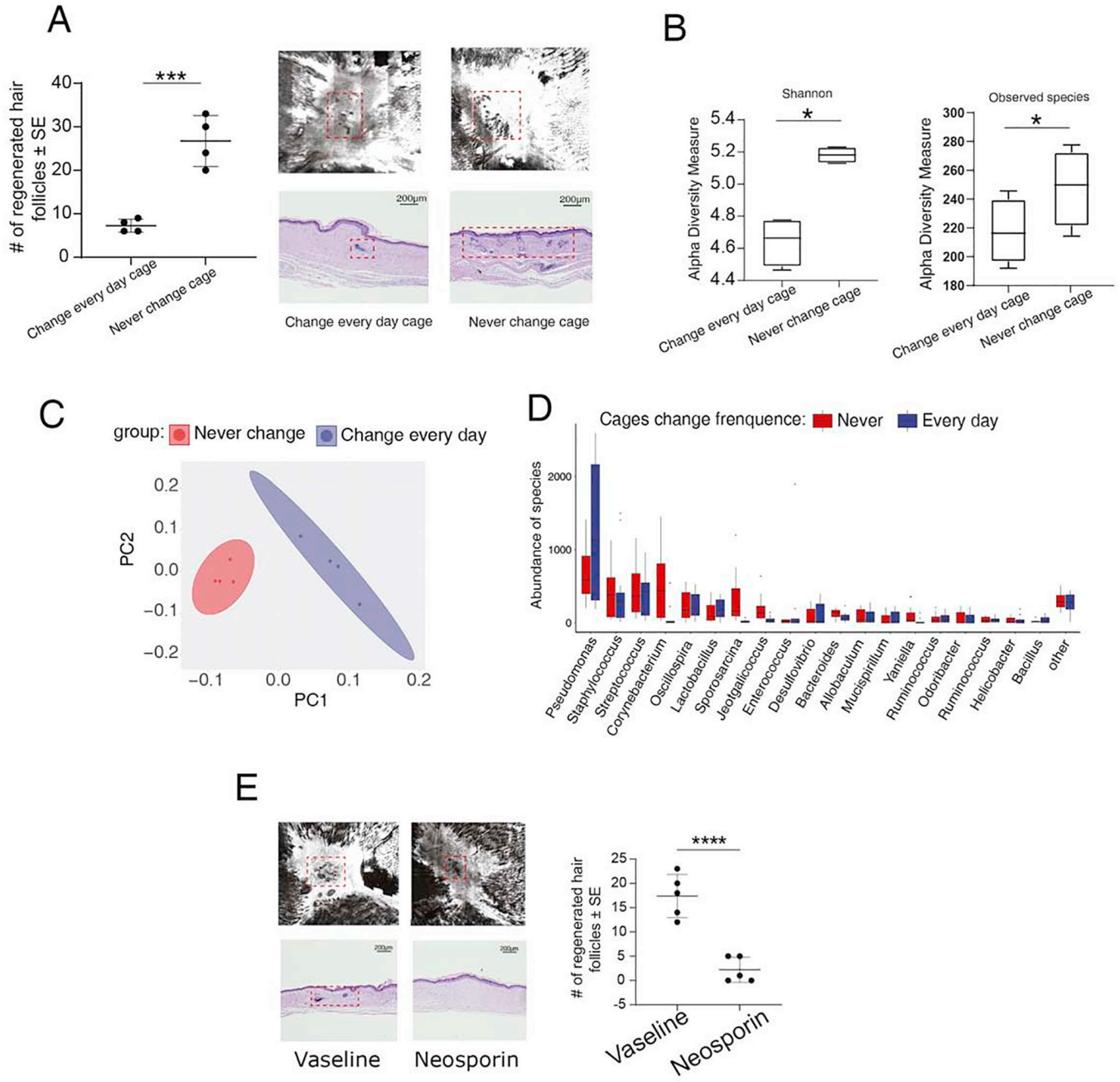

Figure 2. Reducing skin commensal microbiota inhibits WIHN.

(A) WIHN of bedding change every day caged (CED) mice was significantly less than bedding never change caged (NC) mice as detected by CLSM (right top), H&E staining (right bottom), and quantification (left). (n=4 independent animals per group). **(B)** Among CED mice, microbiota α-diversity (Shannon and Observed species) was significantly lower than in NC mice. (n=4 independent animals per group). **(C)** PCA based on microbiota β-diversity shows separate clustering of CED mice and NC mice. (n=4 independent animals per group). **(D)** Absolute value of taxonomic classifications at genus level of 16S rDNA sequence from skins of CED and NC mice. (n=4 independent animals per group). **(E)** WIHN

is lower after topical Neosporin treatment compared to control mice as detected by CLSM (top left), H&E staining (bottom left), and quantification (right). The red dotted line frames regenerative hair follicles. (n=5 independent animals per group). Representative data from 2~3 independent experiments are shown. Boxplot graphs indicated the value of minimum, first quartile, median, third quartile, and maximum. Scatter plots and histogram graphs indicated means ± SEM; Paired Student *t-test* was used to compare statistical difference, $*P < 0.05$, $**P < 0.01$, $***P < 0.001$, and $****P < 0.0001$.

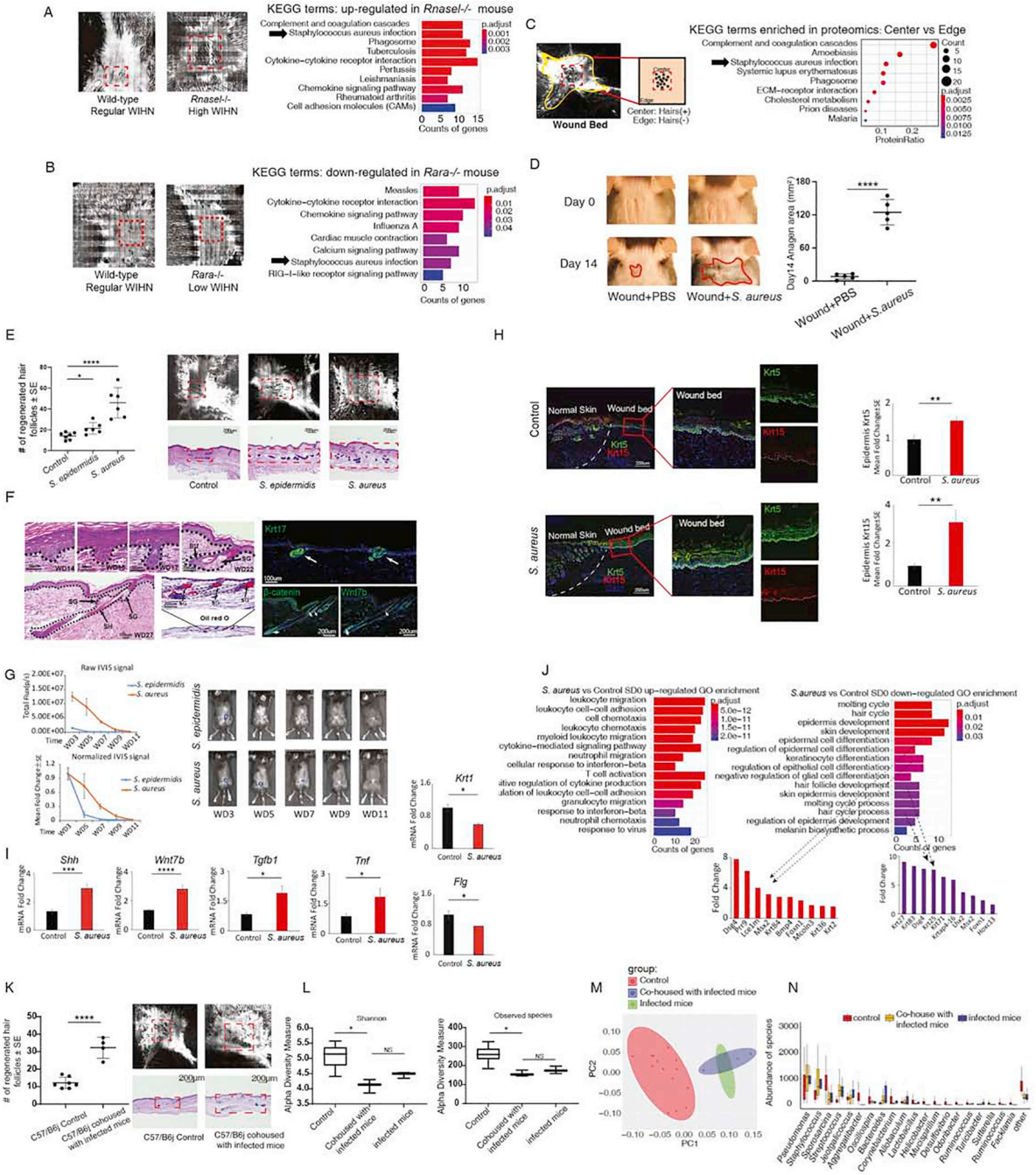

Figure 3. *Staphylococcus aureus* induce WIHN.

(A) Elevated WIHN in *Rnasel*$^{-/-}$ mice (left) correlates with *S. aureus* gene ontology category of gene expression in Kyoto Encyclopedia of Genes and Genomes (KEGG) enrichment analysis of the top 500 differentially expressed genes of *Rnasel*$^{-/-}$ versus WT mice SD0 wound beds (right). **(B)** As in A, except comparing wild type (higher WIHN) versus *Rara*$^{-/-}$ (lower WIHN) **(C)** Schematic of hair neogenesis preferential localization to wound center (high WIHN) rather than edge (low WIHN) (left). Proteomic KEGG enrichment analysis of SD0 wound center versus wound edge in wild type mice (right), also

showing the *S. aureus* category. **(D)** *S. aureus* treatment of mouse skin induces entry to the anagen hair growth phase more than vehicle treated mice after 14 days (left). Anagen hair follicle surface area is marked by red lines and quantified (right). (n=5 independent animals per group). **(E)** WIHN in *S. epidermidis* and *S. aureus* treated mice was significantly more than control mice as detected by CLSM (right top), H&E staining (right bottom), and quantification (left). (n=6–7 independent animals per group). **(F)** The de novo hair follicles induced by *S. aureus* mimic embryonic hair follicle development pattern with high Krt17 in hair germs. After morphogenesis, follicles appropriately express β-catenin, and Wnt7b in the bulge and bulb regions, with intact sebaceous gland (Oil red O). Abbreviations: BU: bulge, SG: sebaceous gland, HS: hair shaft. **(G)** *S. aureus* persisted in the skin longer than *S. epidermidis* (right) as quantified by in vivo bioluminescent signals total flux (p/s) (left up) and normalized flux (p/s) (left bottom). (n=6 independent animals per group). **(H)** Krt5 and Krt15 expression in epidermis of *S. aureus* treated mice, as normalized to adjacent normal skin were significantly higher than in control mice as detected by immunofluorescence staining and quantification. The dotted white line marks the boundary between the wound and normal tissue, and the white scale bar is 200um. (n=3 independent animals per group). **(I)** Higher mRNA expression of hair regeneration signaling (*Wnt7b*, *Shh, tgfb1*), inflammatory cytokines (*Tnf*) with lower expression of keratinocytes differentiation markers (*Flg*, *Krt1*) in *S. aureus* versus control treated mice. (n=3 independent animals per group). **(J)** GO enrichment analysis of the top and bottom 500 differentially expressed genes illustrate higher immune and decreased differentiation categories in *S. aureus* versus control treated mice SD0 wound beds. Inset are selected genes from notable categories (n=3 independent animals per group). **(K)** WIHN in WT mice co-housed with *S. aureus* infected mice are significantly higher than control mice as detected by CLSM (right top), H&E staining (right bottom), and quantification (left). (n=4–7 independent animals per group). **(L)** Microbiota α-diversity based on Shannon and Observed species of mice co-housed with *S. aureus* infected mice and *S. aureus* infected mice themselves were lower than in control mice. (n=3–14 independent animals per group). **(M)** PCA based on Microbiota β-diversity shows clustering of mice co-housed with *S. aureus* infected mice and *S. aureus* infected mice apart from control mice. (n=3–14 independent animals per group). **(N)** Taxonomic classifications at genus level of 16S rDNA sequence from the skins of C57/B6j control mice, C57/B6j co-housed with *S. aureus* infected mice, and *S. aureus* infected mice. (n=3–14 independent animals per group). Representative data from 2~3 independent experiments are shown. Boxplot graphs indicated the value of minimum, first quartile, median, third quartile, and maximum. Scatter plots and histogram graphs indicated means ± SEM; Paired Student *t-test* was used to compare statistical difference, $*P < 0.05$, $**P < 0.01$, $***P < 0.001$, and $****P < 0.0001$. “NS” indicates no significant difference.

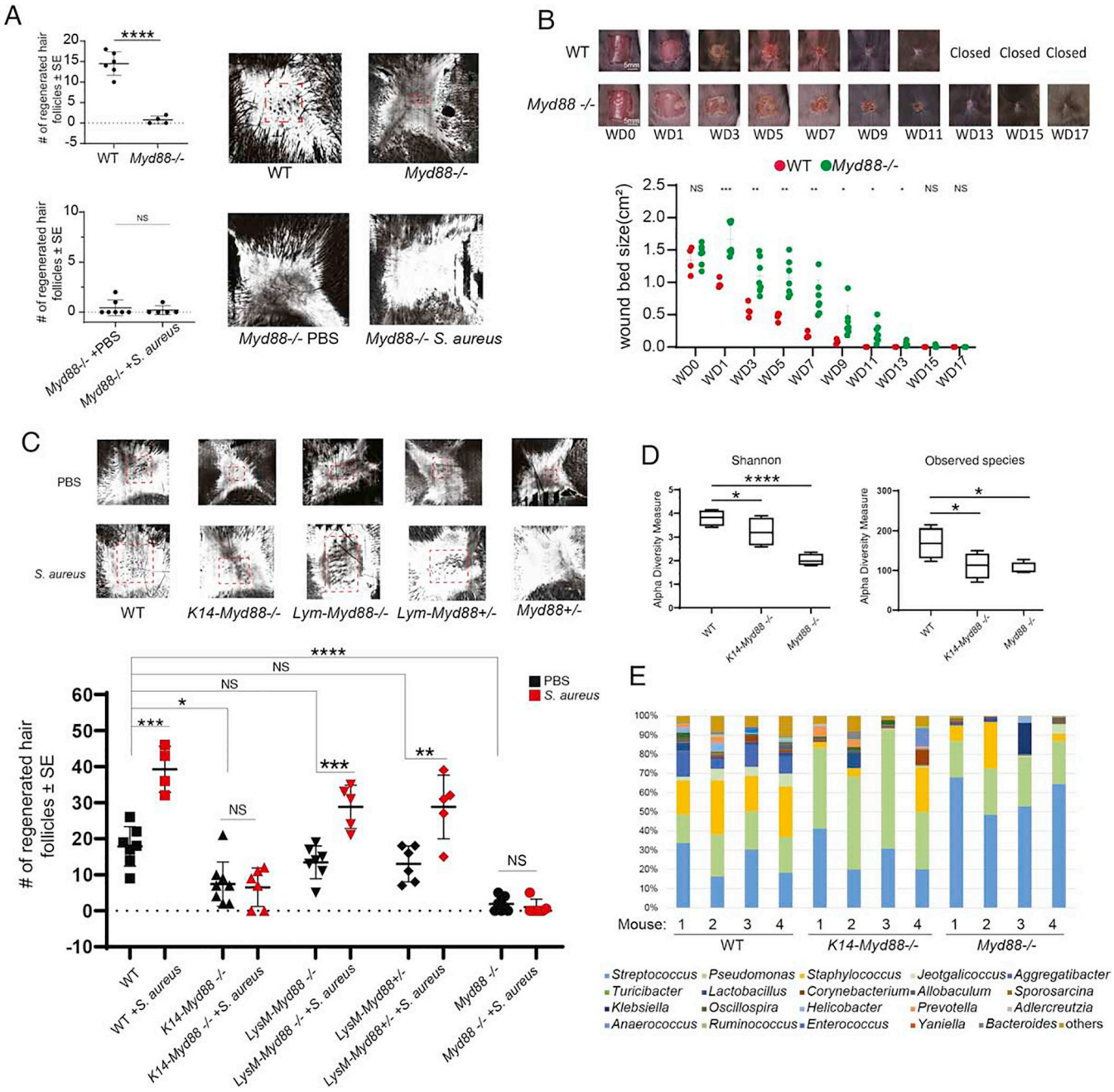

Figure 4. Bacteria induced WIHN is mediated by MyD88 signaling in keratinocytes.

(A) WIHN in *Myd88*$^{-/-}$ mice was significantly less than in WT mice (top) and could not be induced by *S. aureus* treatment (bottom). (n=4–7 independent animals per group). **(B)** The wound closure speed of *Myd88*$^{-/-}$ mice was significantly slower than the WT mice as per photos (top) and quantification (bottom) (n=4–7 independent mice per group). **(C)** WIHN in *S. aureus* treated or untreated WT, *K14-Myd88*$^{-/-}$, *LysM-Myd88*$^{-/-}$, *LysM-Myd88*$^{+/-}$, and *Myd88*$^{-/-}$ mice (top) with quantification (bottom). WIHN in *K14-Myd88*$^{-/-}$ mice was significantly less than WT mice and unresponsive to *S .aureus*. (n=4–10 independent animals per group). **(D)** Microbiota α-diversity (Shannon and Observed species) was

significantly lower than in *K14-Myd88*$^{-/-}$ and *Myd88*$^{-/-}$ mice versus WT mice. (n=4 independent animals per group). **(E)** Percentage of taxonomic classifications at genus level of 16S rDNA sequence from skins of WT, *K14-Myd88*$^{-/-}$, and *Myd88*$^{-/-}$ mice demonstrate that *Pseudomonas* or *Streptococcus* increased while other bacteria, including *Staphylococci* (yellow), decreased in Myd88 deficient mice (n=4 independent animals per group). Representative data from 2~3 independent experiments are shown. Scatter plots and histogram graphs indicated means ± SEM; Paired Student *t-test* was used to compare statistical difference, *$P < 0.05$, **$P < 0.01$, ***$P < 0.001$, and ****$P < 0.0001$. “NS” indicates no significant difference.

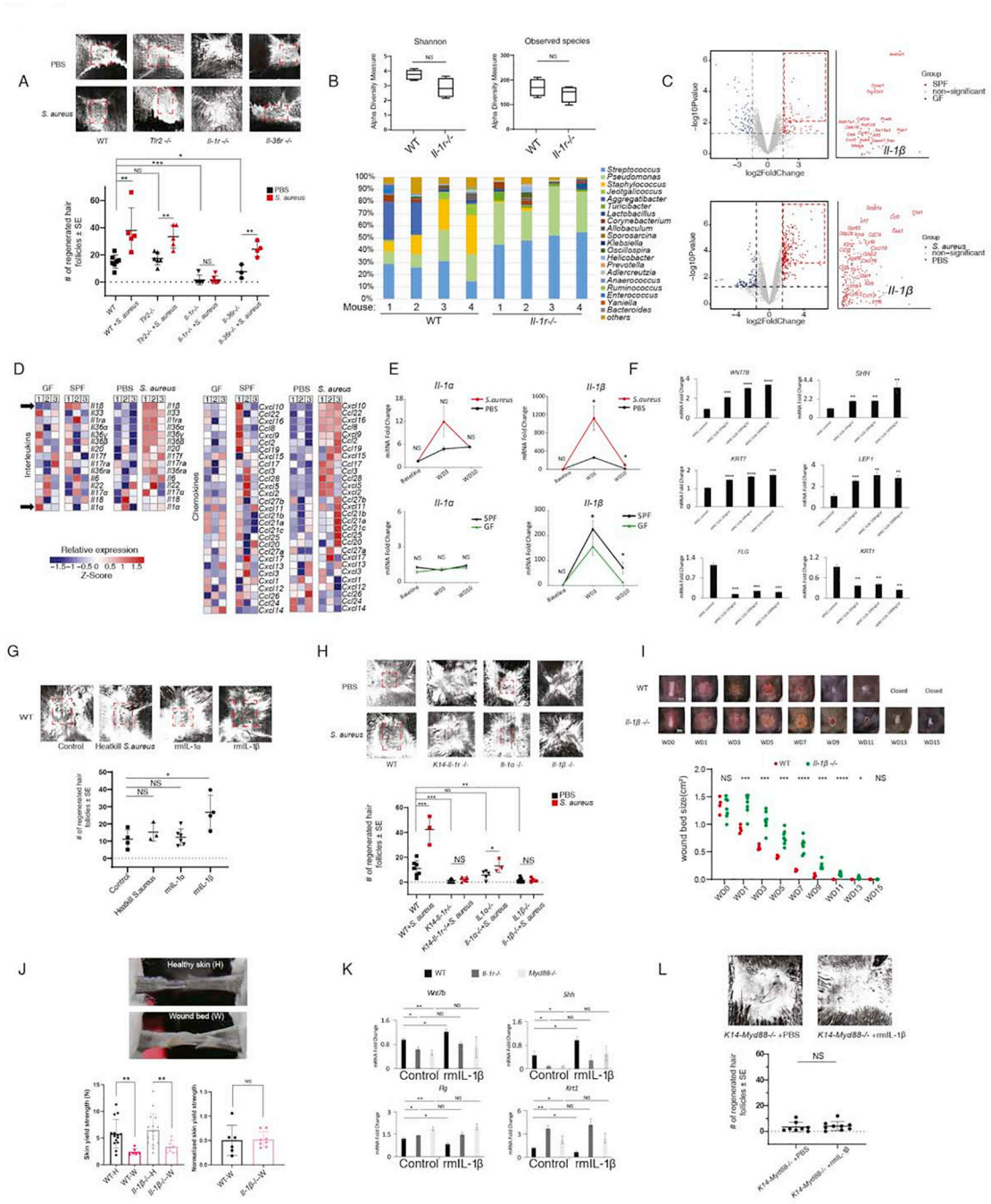

Figure 5. IL-1β-IL-1R signaling in keratinocytes is the primary MyD88 stimulus to promote WIHN.

(A) WIHN in *S. aureus* treated or untreated WT, *Tlr2*$^{-/-}$, *Il-1r*$^{-/-}$, and *Il-36r*$^{-/-}$ mice (top) with quantification (bottom). WIHN in *Il-1r*$^{-/-}$ mice was significantly less than WT mice and unresponsive to *S. aureus*. (n=3–7 independent animals per group). **(B)** Among *Il-1r*$^{-/-}$ mice, microbiota α-diversity (Shannon and Observed species) was not significantly different from WT mice. (n=4 independent animals per group). Percentage of taxonomic classifications at genus level of 16S rDNA sequence from skins of WT and *Il-1r* $^{-/-}$ mice

demonstrate that *Pseudomonas* and *Streptococcus* increased while other bacteria including *Staphylococcus* (yellow) decreased in IL-1 deficient mice (n=4 independent animals per group). **(C)** Differentially expressed genes presented by volcano plot demonstrate that *Il-1β* is one of the most significantly up-regulated genes shared by SPF and *S. aureus* treated mice. (n=3 independent animals per group). **(D)** Relative microarray mRNA expression of interleukins and chemokines in GF, SPF, PBS treated, and *S. aureus* treated mice SD0 wound bed tissues demonstrate that *Il-1β* correlates with WIHN. (n=3 independent animals per group). **(E)** qRT-PCR mRNA expression of *Il-1α* and *Il-1β* of GF, SPF, PBS treated, and *S. aureus* treated mice at baseline (unwounded), WD3, and WD10 confirm that *Il-1β* correlates with WIHN. (n=3 independent animals per group). **(F)** qRT-PCR mRNA expression show increases of hair regeneration markers (*Wnt7B*, *Shh*, *Lef1*) and stem cell marker (*Krt7*) with decreases in keratinocyte differentiation markers (*Flg*, *Krt1*) in rhIL-1β treated human foreskin keratinocytes (HFKC) compared to vehicle. (n=2–4 independent human samples per group). **(G)** WIHN in rmIL-1β treated mice is significantly more than control, heat killed *S. aureus* treated, and rmIL-1α treated mice. (n=3–6 independent animals per group). **(H)** WIHN in *S. aureus* treated or untreated WT, *K14-Il-1r*$^{-/-}$, *Il-1α*$^{-/-}$, and *Il-1β*$^{-/-}$ mice (top) with quantification (bottom). WIHN in *K14-Il-1r*$^{-/-}$ mice and *Il-1β*$^{-/-}$ mice was significantly less than WT mice and unresponsive to *S. aureus*. (n=3–7 independent animals per group). **(I)** The wound closure speed of *Il-1β*$^{-/-}$ mice was significantly slower than the WT mice as per photos (top) and quantification (bottom) (n=4–7 independent mice per group). **(J)** There is no significant difference in WD28 wound bed tensile strength between WT and *Il-1β*$^{-/-}$ mice, both of which are lower than their respective healthy skin (n=6–9 independent mice per group). **(K)** Relative mRNA expression of hair regeneration markers (*Wnt7b*, *Shh*) and keratinocytes differentiation markers (*Flg*, *Krt1*) in rmIl-1β treated, untreated control, *Il-1r*$^{-/-}$, and *Myd88*$^{-/-}$ mice keratinocytes. (n=3 independent animals per group). **(L)** WIHN in rmIl-1β treated *K14-Myd88*$^{-/-}$ mice was the same as control mice (n=8–9 independent animals per group). Representative data from 2~3 independent experiments are shown. Scatter plots and histogram graphs indicated means ± SEM; Paired Student *t-test* was used to compare statistical difference, *$P < 0.05$, **$P < 0.01$, ***$P < 0.001$, and ****$P < 0.0001$. “NS” indicates no significant difference.

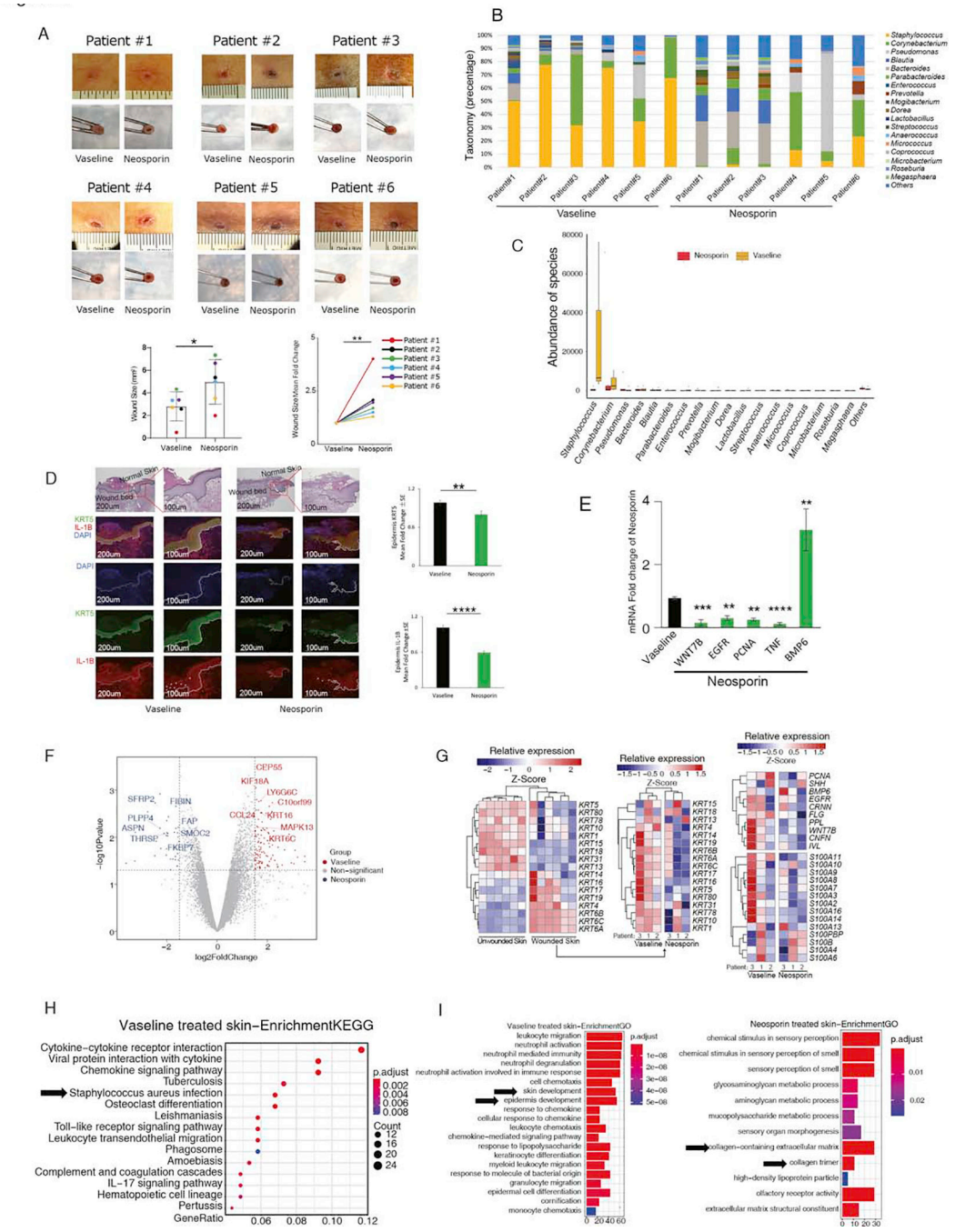

Figure 6. Antibiotics Inhibit Human Wound Healing.

(A) After identical full thickness punch wounds in the same individual, the size of Neosporin treated human wounds were significantly larger than the Vaseline treated control wounds as per photos (top), quantification (left bottom), and intra-individual normalization (right bottom). (n=6 independent human samples per group). **(B and C)** Absolute value (B) and percentage (C) of taxonomic classifications at genus level of 16S rDNA sequence from skins of Vaseline and Neosporin treated patients demonstrate that *Staphylococcus* (yellow) is the bacteria with the biggest difference after antibiotic treatment. (n=6 independent human

samples per group). **(D)** Neosporin delayed wound healing as visualized by hematoxylin and eosin (H&E) staining (left). Neosporin also decreased the expression of KRT5 and IL-1β (indicated by arrow) in the wound bed epidermis as detected by immunofluorescence staining (left) and quantification (right). (n=4 independent human samples per group). **(E)** qRT-PCR mRNA expression analysis of Vaseline and Neosporin treated human wounded skin. (n=3 independent human samples per group). **(F and G)** Microarray mRNA analysis demonstrates that wound associated keratins and chemokines are more highly expressed in Vaseline compared to Neosporin treated skin. (n=3 independent human samples per group). **(H and I)** Gene ontology analysis shows *S. aureus* and Epidermal Development signatures are elevated in Vaseline compared to Collagen categories in Neosporin treated samples. (n=3 independent human samples per group). Representative data from 2 independent experiments are shown. Scatter plots and histogram graphs indicated means ± SEM; Paired Student *t-test* was used to compare statistical difference, $*P < 0.05$, $**P < 0.01$, $***P < 0.001$, and $****P < 0.0001$.

KEY RESOURCES TABLE

REAGENT or RESOURCE	SOURCE	IDENTIFIER
Experimental models: organisms/strains		
C57BL/6j	Jackson Laboratory	Stock No: 000664
Tlr2$^{-/-}$	Jackson Laboratory	B6.129-Tlr2tm1Kir/J Stock No: 004650
Il-1r$^{-/-}$	Jackson Laboratory	B6.129S7-Il1r1tm1Imx/J Stock No: 003245
Myd88$^{-/-}$	Jackson Laboratory	B6.129P2(SJL)-Myd88tm1.1Defr/J Stock No:009088
LysM-cre	Jackson Laboratory	B6.129P2-Lyz2tm1(cre)Ifo/J Stock No:004781
Myd88$^{fl/fl}$	Jackson Laboratory	B6.129P2(SJL)-Myd88tm1Defr/J Stock No: 008888
Il-36r$^{-/-}$	Amgen	NA
K14-Il-1r$^{-/-}$	Nathan Archer (Johns Hopkisn University)	NA
K14-Myd88$^{-/-}$	Nathan Archer (Johns Hopkisn University)	NA
Il-1α$^{-/-}$	Yoichiro Iwakura (University of Tokyo)	NA
Il-1β$^{-/-}$	Yoichiro Iwakura (University of Tokyo)	NA
Il-17a/f$^{-/-}$	Yoichiro Iwakura (University of Tokyo)	NA

REAGENT or RESOURCE	**SOURCE**	**IDENTIFIER**
Bacterial and virus strains		
Staphylococcus aureus NRS384	BEI Resources	N/A
Staphylococcus epidermidis Xen43	BEI Resources	N/A
Staphylococcus xylosus NKA352	This paper	N/A
Streptococcus pyogenes Xen20	PerkinElmer	N/A
Pseudomonas aeruginosa Xen41	PerkinElmer	N/A

REAGENT or RESOURCE	SOURCE	IDENTIFIER
Oligonucleotides		
TaqMan Murine *Krt15* primers	Applied Biosystems	ID: Mm00492972_m1
TaqMan Murine *Wnt7b* primers	Applied Biosystems	ID: Mm01301717_m1
TaqMan Murine *Flg* primers	Applied Biosystems	ID: Mm01716522_m1
TaqMan Murine *Arg1* primers	Applied Biosystems	ID: Mm00475988_m1
TaqMan Murine *Nos2* primers	Applied Biosystems	ID: Mm00440502_m1
TaqMan Murine *Krt1* primers	Applied Biosystems	ID: Mm00492992_g1
TaqMan Murine *Shh* primers	Applied Biosystems	ID: Mm00436528_m1
TaqMan Murine *Il-1α* primers	Applied Biosystems	ID: Mm00439620_m1
TaqMan Murine *Il-1β* primers	Applied Biosystems	ID: Mm00434228_m1
Other primers	Table S1	NA

REAGENT or RESOURCE	SOURCE	IDENTIFIER
Biological Samples		
Healthy adult popliteal fossae skins	This paper	N/A
Discarded neonatal foreskins	This paper	N/A

REAGENT or RESOURCE	SOURCE	IDENTIFIER
Experimental Models: Cell Lines		
Human keratinocytes	This paper	N/A
Mouse keratinocytes	This paper	N/A

REAGENT or RESOURCE	SOURCE	IDENTIFIER
Critical Commercial Assays		
RNeasy Mini Kit	Qiagen	74106
High-Capacity cDNA Reverse Transcription Kit	Applied Biosystems	4368813
Taqman Gene Expression Master Mix	Applied Biosystems	4369016
Mouse Pan T cell Isolation Kit	Miltenyi Biotec	130-095-130

REAGENT or RESOURCE	SOURCE	IDENTIFIER
Antibodies		
Krt5 (Chicken)	Biolegend	905901
Krt5(Rabbit)	Abcam	Ab52635
Krt15 (Rabbit)	Sigma	HPA023910
β-Catenin (Rabbit)	Abcam	Ab6302
IL-1 β (Rabbit)	Abcam	Ab2105
Wnt7b(Rabbit)	Abcam	Ab155313
Krt17(Rabbit)	Abcam	Ab53707
F4/80(Rat)	Abcam	Ab6640
Alexa Fluor® 488 Anti-Mouse IgG (Goat)	Invitrogen	A-11001
Alexa Fluor® 488 Anti-Rabbit IgG (Goat)	Invitrogen	A-11008
Alexa Fluor® 594 Anti-Rabbit IgG (H+L) (Goat)	Invitrogen	A-11037
Alexa Fluor® 488 Anti-Chicken IgG (Goat)	Invitrogen	A-11039
Alexa Fluor® 488 Anti-Rat IgG (Goat)	Invitrogen	A-11006
Anti-mouse Viobility Viogreen	Miltenyi Biotec	130109814
Anti-mouse CD11b Apc-Cy7	BD Biosciences	557657 Clone: M1/70
Anti-mouse CD45 Vioblue	Miltenyi Biotec	130118953 Clone:30F11
Anti-mouse CD3 PE-cy7	BD Biosciences	560591 Clone: 17A2
Anti-mouse CD4 BV 650	Biolegend	100545 Clone: RM4–5
Anti-mouse TCRgd Per-cp Vio700	Biolegend	118117 Clone:GL3
Anti-mouse Ly6C FITC	BD Biosciences	553104 Clone:AL-21
Anti-mouse Ly6G PE	Biolegend	127607 Clone:1A8
Anti-mouse F4/80 APC	Biolegend	123116 Clone:BM8
Anti-mouse CD86 Per-cp cy5.5	Biolegend	105027 Clone:GL-1
Anti-mouse CD206 PE-cy7	Biolegend	141719 Clone:C068C2
Anti-mouse CD8 FITC	BD Biosciences	553030 Clone:53-6.7
Anti-mouse Il-17 PE	Biolegend	506903 Clone:TC11-18H10.1
Anti-mouse Il-22 APC	BD Biosciences	554714 Clone:Poly5164

REAGENT or RESOURCE	SOURCE	IDENTIFIER
Deposited Data		
16S rRNA-seq data	NCBI SRA	PRJNA665993 and PRJNA665992
Microarray data	NCBI GEO	GSE158613, GSE158614, and GSE158616

REAGENT or RESOURCE	SOURCE	IDENTIFIER
Software and algorithms		
Fiji (ImageJ)	NIH	https://fiji.sc
GraphPad Prism	GraphPad Software, Inc	https://www.graphpad.com
QIIME 2	QIIME 2 development team	https://qiime2.org/
R version 4.0.2	R	https://www.r-project.org/
ggplots2	R package	https://ggplot2.tidyverse.org
limma	R package	https://bioconductor.org/packages/release/bioc/html/limma.html
clusterProfiler	R package	https://bioconductor.org/packages/release/bioc/html/clusterProfiler.html